Analysis of Ant Neck Tissue Using Scanning Electron Microscopy Imaging (SEM)

Undergraduate Honors Research Thesis

Presented in Partial Fulfillment of the Requirements for
Graduation with Honors Research Distinction in the
Department of Mechanical and Aerospace Engineering at
The Ohio State University

By

Hiromi Tsuda

2015

Undergraduate Program in Mechanical and Aerospace Engineering

Nanoengineering and Biodesign Laboratory

Thesis Committee:

Advisor: Dr. Carlos Castro

Dr. Blaine Lilly

Dr. Sandra Metzler

Abstract

Ants are known for their ability to carry extremely heavy loads, upwards of 1,000 times their own weight. Though the mass towed by the ant is distributed over six legs, the entirety of load must pass through its neck. Therefore, the long-term goal of this work is to understand the material and structure design principles of the ant neck joint that enable its mechanical function. Our recent mechanical studies of the neck joint of an Allegheny Mound Ant revealed that the neck membrane has an elastic modulus of 230±140MPa and an ultimate failure stress of 37 MPa, which is consistent with locust wing membrane of approximately 52 MPa. Since the material properties are similar to other insect systems, we suspect that both macroscopic and microscopic structural mechanisms contribute to extreme load-bearing capabilities of ants. Scanning electron microscopy (SEM) of failed specimens revealed the critical point for failure is at the transition between the soft membrane of the neck and the hard exoskeleton of the head. This work focuses on exploring the microstructure mechanisms that contribute to enhancing the strength of this interface. The neck joint of carpenter ants will be sectioned and imaged using SEM. In order to achieve precise sections of the neck joint, the specimens are first embedded in acrylic plastic resin, then machined using 1/64" carbide end mills on a milling machine. Once the neck is successfully exposed, the specimen is imaged. The goal of this research is to image the material, surface, and interface microstructure with improved resolution to form the basis of a micromechanical model. This will aid in the understanding of the mechanical function of the ant neck joint.

Dedication

This study is dedicated to my family and friends.

Acknowledgements

I would like to thank my advisor, Dr. Carlos Castro for all the continuous encouragements and positive feedback he gave me throughout my study at the Ohio State University, and for welcoming me into his research. I would also like to thank him for going above and beyond as an advisor, giving me not only abundant research advice but also providing me with invaluable life lessons.

I would also like to thank Dr. Blaine Lilly for taking the time to serve on my undergraduate research defense committee, for introducing me to the ant neck study, and for being a wonderful advisor to the ant neck research.

Additionally, I want to thank the following people: Dr. Noriko Katsube for giving me the introduction to Dr. Castro; Vivianne Owino with whom I originally started my research under; and Vienny Nguyen for all the advice she gave me to get started. Also, I would like to send my gratitude to all the people who helped me throughout this study, including: George Keeney at the OSU Greenhouse, Cameron Begg at CEMAS, and Walter Green at the Scott Lab Student Machine Shop.

A special thank you goes to AC Taylor and Leon, who provided me with endless support and motivation throughout my studies.

Finally, I thank God for being my strength and giving me guidance throughout my time at the Ohio State University.

Table of Contents

List of Figures

Chapter 1. Introduction

Ants are known for their ability to carry extremely heavy loads, upwards of 1,000 times their own weight [1]. As seen in Figure 1A and B below, a single worker ant weighing approximately 6mg uses its mandible to carry a dead baby bird of approximately 7g by its feet, off the side of a table. This is comparable to an average human adult lifting a 737 commercial airplane off the edge of a cliff [3]. Though the mass towed by the ant is distributed over six legs and tarsi (feet), the entirety of load must pass through its neck. This ability inspired the study on how material and structural design relates to the mechanical function of the ant's neck joint.

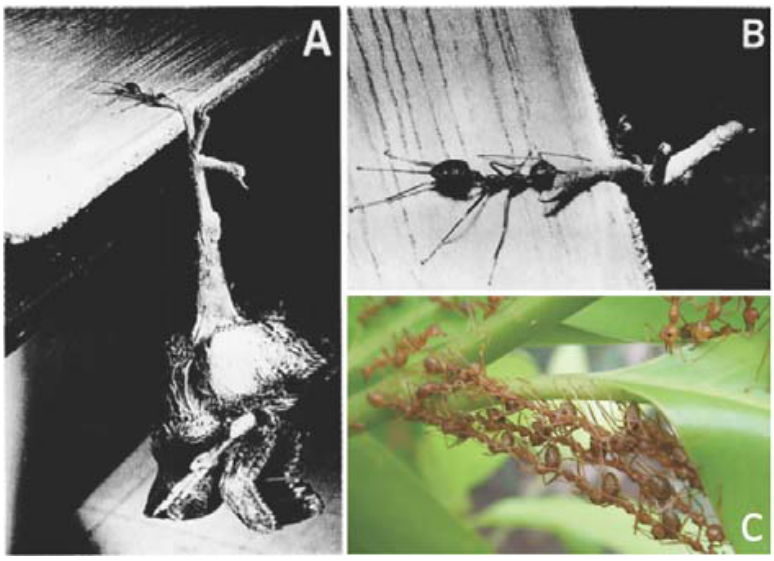

Figure 1: *O. longinoda* worker holding a dead bird ~1000 times its own weight (A) and (B) [1]. Nest construction by *O. smaragdina* workers (C) [2].

Vienny Nguyen, a former Ohio State University graduate student, chose to focus her research specifically on the neck joint of the ant, as the neck has the ability to withstand these incredibly high tensile stresses, despite having a soft neck

membrane. One key finding from her research was that the critical point for failure in the ant neck is at the transition between the soft tissue material of the neck and the hard exoskeleton of the head.

Nguyen and her advisor Dr. Blaine Lilly (Associate Professor, MAE) designed and constructed a custom centrifuge device to test mechanical behaviors of the ant, such as the tensile strength of the neck joint.

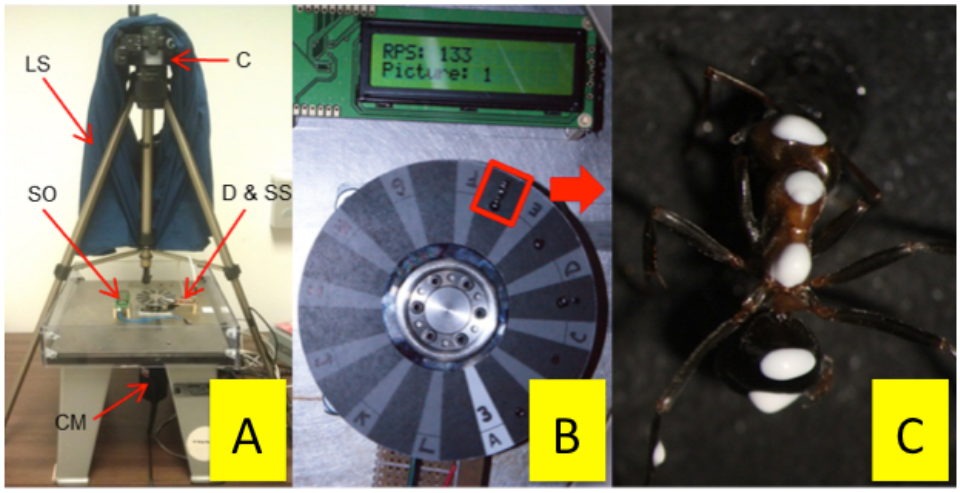

Figure 2: (A) Custom-built centrifuge device with a high speed camera mounted at the top directly above centrifuge platform. (B) Circular centrifuge platform that spun at specified speeds shown in the display. (C) Reference markers placed along the body of the specimen. [4]

Their studies focused on the ant species, *Formica exsectoides*, also known as Allegheny Mound Ants, which were collected locally. Live ant specimens were attached to the centrifuge platform by the head and spun around at specified speeds to simulate tensile forces acting along the neck, as seen in Figure 2A and B. A high-speed camera captured images of the ant in motion, which provided displacements of reference markers earlier placed on the ant, labeled as C in Figure 2A above. The resulting data from the mechanical testing, such as ones seen in Figure 3 below,

helped identify key material properties of the ant neck joint such as the elastic modulus.

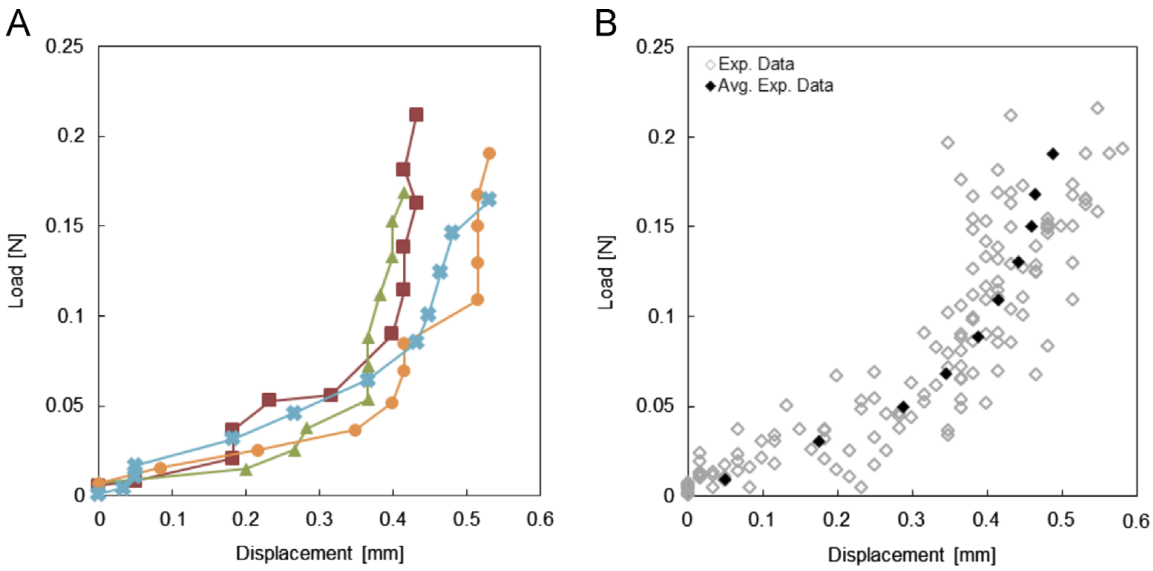

Figure 3: (A) Sample datasets showing a non-linear relationship between applied load and displacement. (B) Aggregate data and averaged dataset used for the material properties definition for FE analysis. [4]

The data allowed them to estimate the elastic modulus of the soft tissue in the neck joint to be 230 ± 140MPa and they estimated an ultimate failure stress of 37MPa [4]. These properties taken as a result of the mechanical testing are consistent with material properties of other insects such as the locust wing membrane, consisting of an ultimate failure stress of approximately 52MPa [13]. This closeness in rupture strength could suggest that the failure mechanisms could be similar across different species of insects.

To study the interface of the rupture point, Finite Element Analysis (FEA) was done to simulate a 3D model of the ant neck joint. In this way, Nguyen was able to determine that the critical stress concentration is located between the soft neck

membrane and the head exoskeleton, upon applied loading [4]. Figure 4 below shows a cross-sectional view of solely the neck region. On the right is the close-up view of the stress concentration within the neck joint.

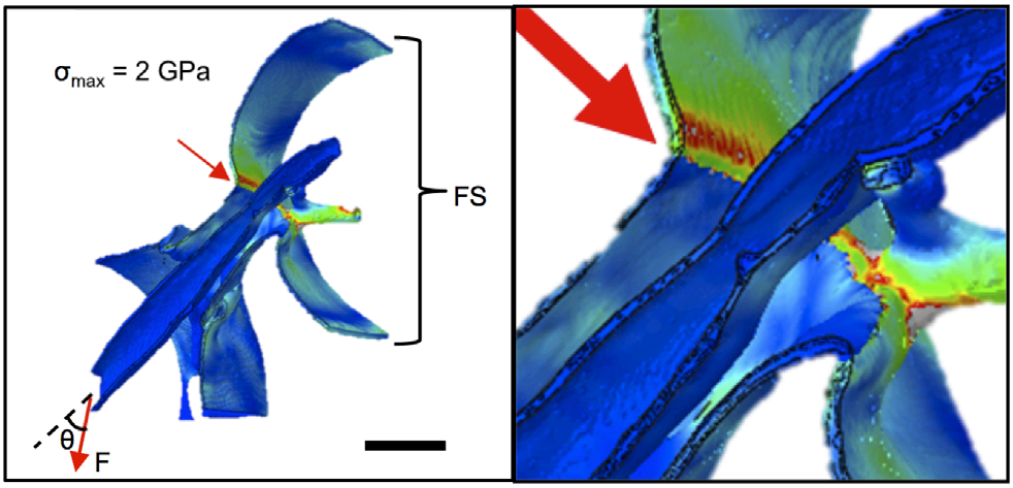

Figure 4: Left -- cross-section of 3D FE model max principal stress contour plot; right -- detail view of stress concentration located at the transition between the neck membrane and the head exoskeleton. F - applied load; FS - fixed surface; θ - load angle away from the neck axis. Scale bar is 200 μm. [4]

As seen in the 3D simulations above, the ant neck region contains a mating interface between soft tissue (esophagus) and hard tissue (thorax and head), which would normally be expected to be a weak region. However, the ant neck is able to transfer surprisingly high tensile stresses without separating at this interface. The average applied load upon rupture was 0.33N (ultimate stress of 37MPa), which is equivalent to over 5,000 times the typical mass of an *Formica exsectoides* ant. To further investigate this ability, Scanning Electron Microscopy (SEM) images of ruptured specimen were taken, as seen in Figure 5 below.

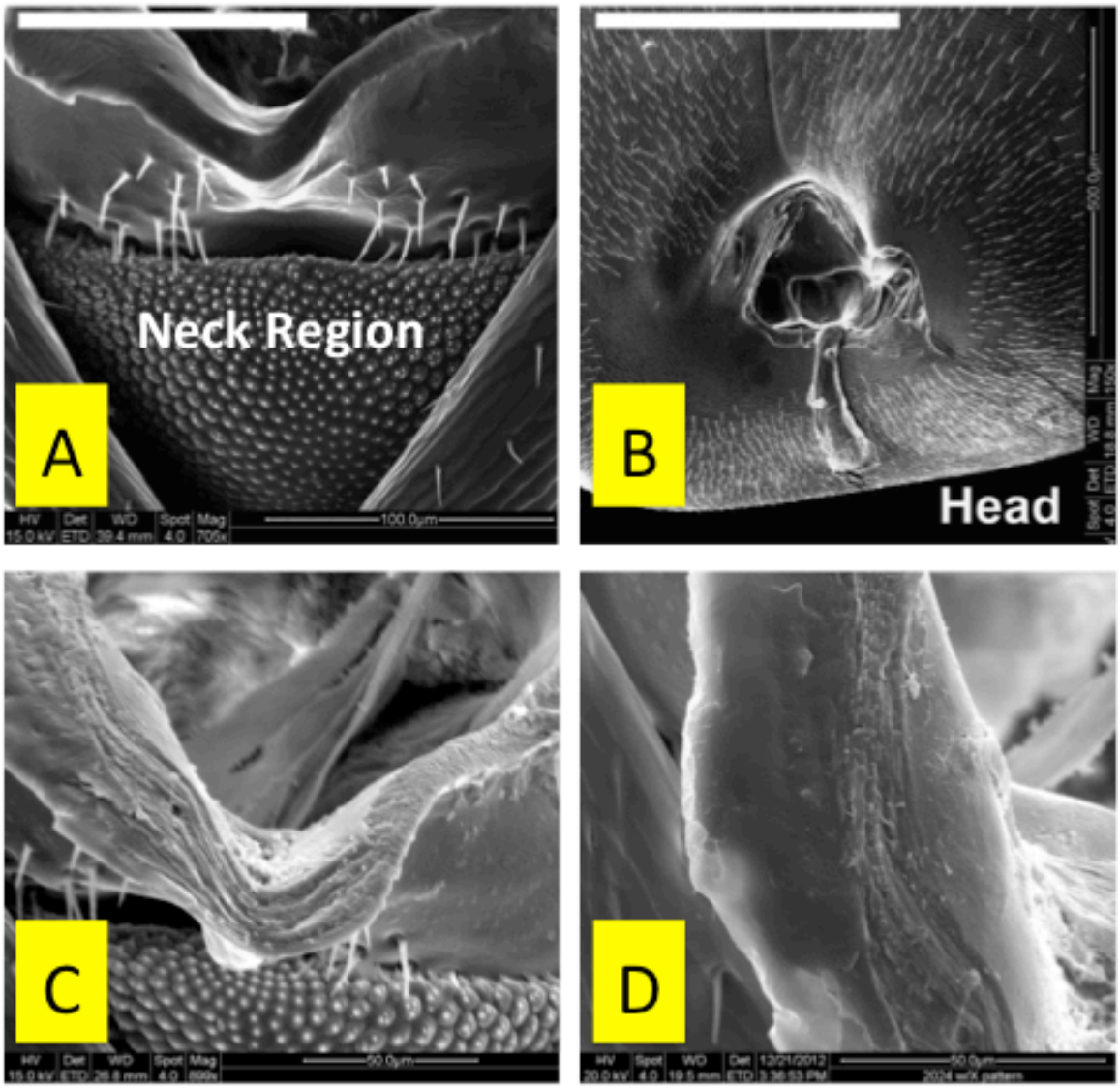

Figure 5: (A) SEM of a ventral view of a ruptured neck of *F. exsectoides* showing proprioceptors on the smooth membrane region and an armored region, scale bar: 100 µm. (B) SEM of posterior view of ruptured neck region on the head, scale bar: 500 µm. (C) SEM of ruptured specimen with graded structure of interface between soft and hard material. (D) Closer look at the interface of Figure 5C. [4]

These SEM images of the ruptured specimen also pointed towards a possible stepped-shaped graded structure of interface between the hard and soft tissue that may contribute to the adhesion strength between the two dissimilar materials. As seen particularly in Figure 5D, approximately a 9-step interface could be estimated.

Following Nguyen, OSU graduate student Vivianne Owino under Dr. Noriko Katsube (Professor, MAE), ran simulations in Abaqus, a Finite Element Analysis (FEA) tool to analyze the stress concentrations seen in the ant neck joint. Owino created numerous two-dimensional models of the ant neck joint to approximate locations and magnitudes of critical stresses under different loads. The geometry of the two-dimensional model was estimated from preliminary SEM images taken by Nguyen, seen previously in Figure 5. Upon running multiple simulations with varying geometry, it was found that with no stepped-interface (straight, vertical), the stress concentration found at the corners of the interface would be too great to withstand any high tensile loading. The rupture strength of 37MPa would not be possible with non-stepped interface. This revealed a potential mechanism, that the hypothesized stepped interface seen in Figure 6A and B between soft and hard tissue, would be a large contribution to the neck's ability to minimize stress concentrations at the hard-to-soft material transition [5,6]. The multiple steps allowed the interface to distribute stress concentrations to minimize large stresses. For these simulations, the elastic modulus of the soft material was taken to be approximately 233 MPa, which is within the range found by Nguyen, and the hard tissue was assigned a stiffness of 2668 MPa based on literature on various insect-body material properties [7].

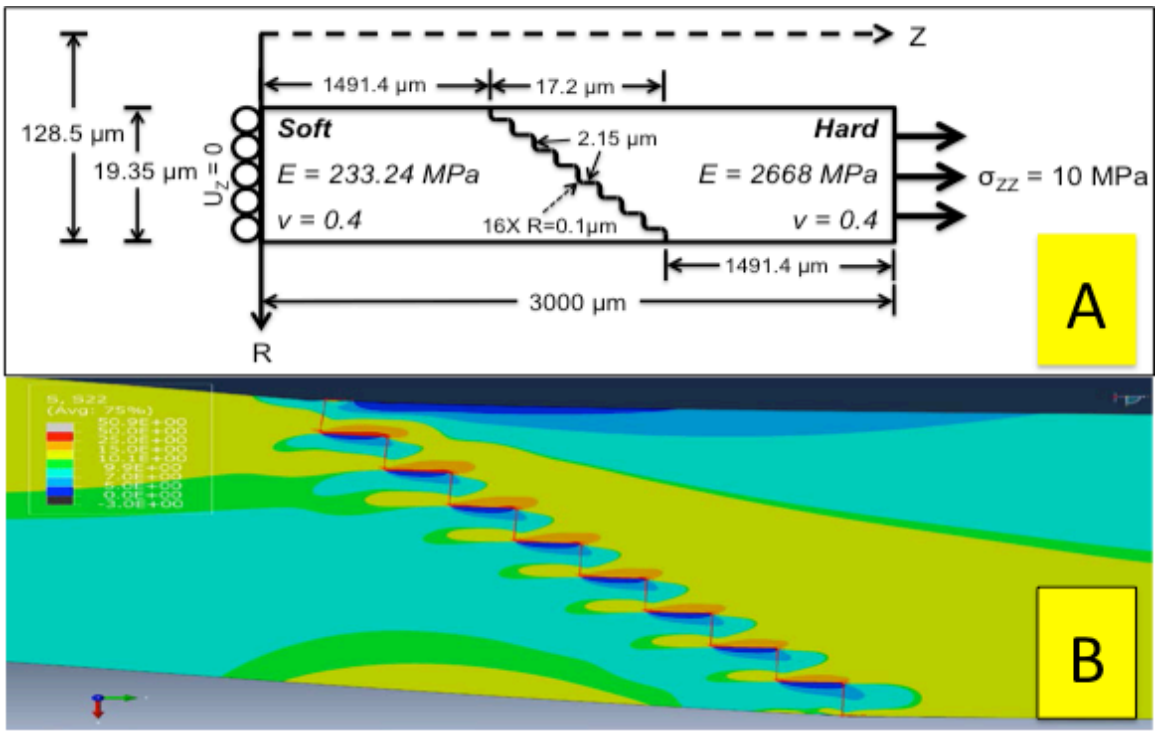

Figure 6: (A) Axisymmetric models of the bi-material hollow cylinders with a 9-step interface. (B) Stress sigma-ZZ contour plot for a 9-step interface using ABAQUS FEA. [6]

1.1 Focus of Thesis

This independent honor's research through Dr. Carlos Castro (Assistant Professor, Mechanical & Aerospace Engineering (MAE)) is an extension of Nguyen and Owino's work, with the aim of investigating the microstructure of the neck joint, in particular the head to neck interface. Through the use of Scanning Electron Microscopy (SEM), the surface and interface microstructure of the ant's neck joint can be studied in depth. More importantly, this may lead to an understanding of how different materials (for example: hard material and soft tissue within the neck) can be mated together to maximize toughness and overall mechanical performance.

1.2 Significance of Research

The ultimate goal of this work is to image the material, surface, and interface microstructure of the ant neck joint with better resolution. This will aid in the understanding of the mechanical function of the ant neck joint. With this understanding of the neck's ability to withstand high tensile loading from an engineering standpoint, it will become possible to reverse engineer this design to apply to various fields such as adhesives.

1.3 Overview of Thesis

This research thesis has five chapters. Chapter 1 gives the introduction to the study and provides some background information. Chapter 2 will focus on background literature review that applies to the study of the ant neck joint and the adhesive quality of the soft-hard membrane interface. Chapter 3 in conjunction with protocols attached in the Appendix will go through the various methodologies involved in capturing the desired high-resolution SEM images. Chapter 4 will delve into the resulting SEM images captured using the two differing methods. The final chapter will give a summary of the study and provides future project plans.

Chapter 2. Literature Review

Background research was done primarily through past research papers and theses written by Vienny Nguyen and Vivianne Owino. These were discussed in the introductory section of this paper. In addition to taking background research from their papers, other literature and journal articles were also reviewed to supplement the perspective on adhesion of composite (dissimilar) materials. The first two papers focus on various insects to introduce the different structures and functions of joints and membranes. Additionally, the literature review will cover composite materials and related crack growth to be able to compare with the rupture mechanism of the ant neck joint. Finally, this section will touch on a methodology similar to what was implemented during the ant neck research.

2.1 *Ultrastructure of the Neck Membrane in Dragonflies* by S.N. Gorb [14]

Studies have been done on the neck of various species of dragonflies, Odanta. Through these studies, they hoped to understand the shape and function of folding cuticle, the external skeletal structure. They used SEM imaging to capture images of the membrane found between hard plates and body sections, as seen in Figure 7 below. As a result, they were able to investigate several hierarchical orders of folds that are present in the neck membrane at different scales. The varying orders of neck membrane folds allow the necks of Odanta to perform various actions such as pitch, roll, and yaw. Some structures allow for high extensibility and some allows the cuticle to be stiffer.

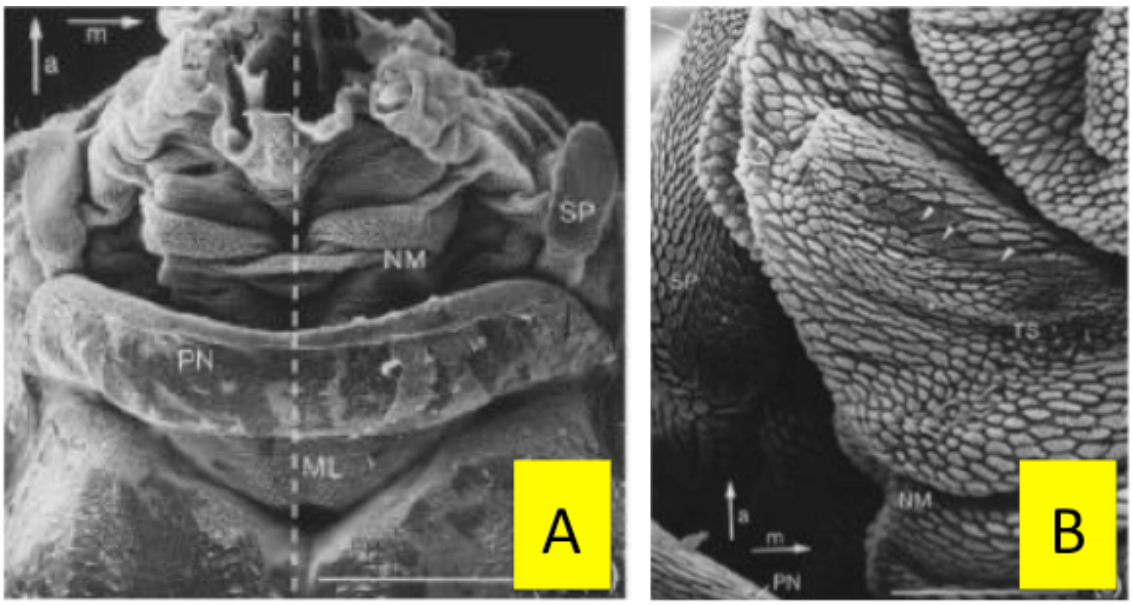

Figure 7: SEM of neck area in damselflies. (A) Dorsal aspect with head removed of *Ischnura elegans;* (B) Dorsal aspect with head removed of *Coenagrion puella.* Scale bars: 380nm (A); 75µm (C) [14]

2.2 *Armored Cuticular Membranes in Brachycera* by S.N. Gorb [15]

In order to understand the structure of the exoskeleton of many insects, in particular the membranous cuticle that stretch between hardened plates, a study was done to correlate the surface structure of the membrane with its function. In this study, various types of flies, also known as *Diptera*, were examined using SEM. The following collage below shows examples of the microstructures observed for various joint types in Figure 8.

These formations captured in the SEM images have several known functions, such as providing structural stability of flexible membranes and vary the frictional forces in contact areas. By varying the direction of deformation and shape of macrostructures, they are able to control frictional forces, allowing them to control their stability. These functions can also be seen in Figure 9 below.

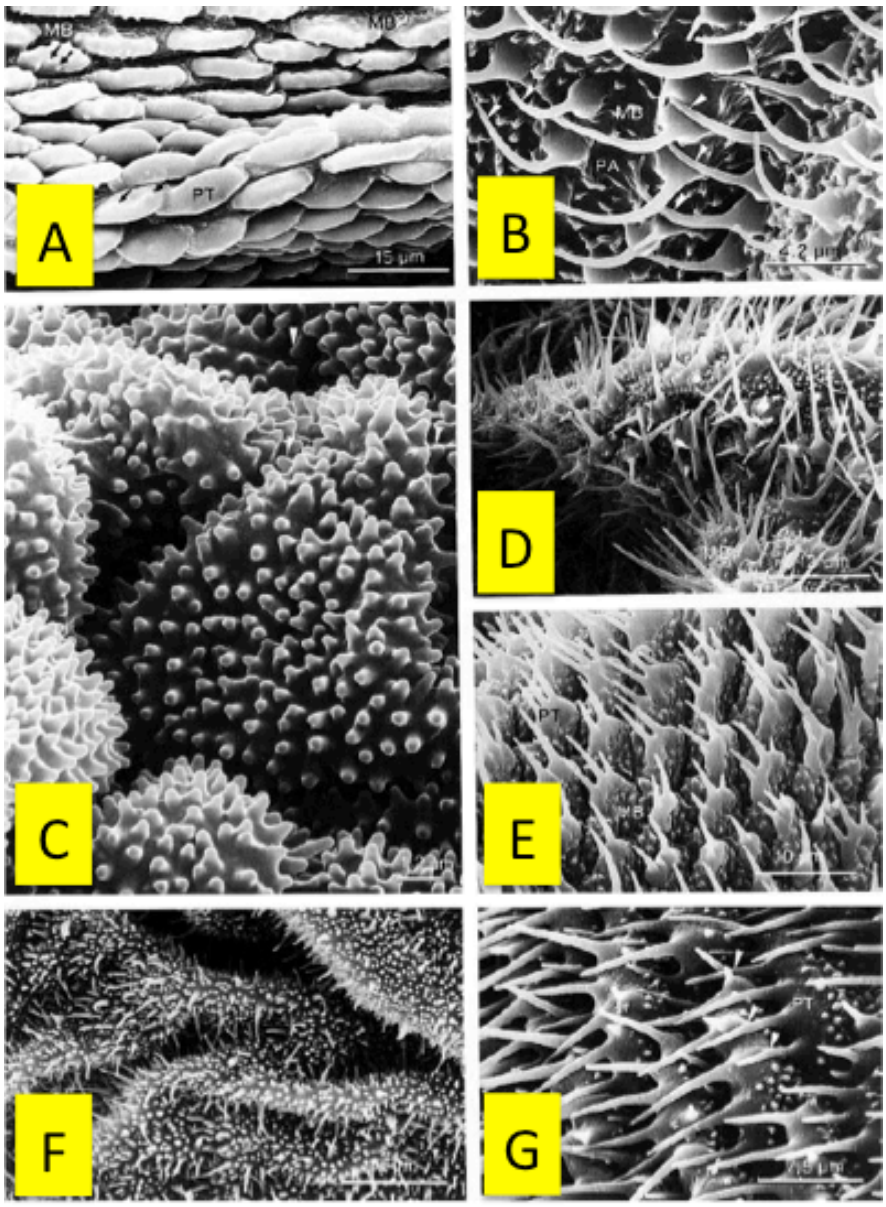

Figure 8: Membranous *cuticle* in *Brachycera*, suborder of Diptera. MB, flexible membrane; PT, microplates; Arrowheads indicate point of contact between *microtrichia*. (A) Microplates of *Statriomys chamaeleon* legs (B) Membrane showing curved, parallel microtrichia of *Lucilia caesar* legs; (C) Short papillae on the prothorax-neck membrane of *Tabanus bovinus*; (D) membrane of the hip-leg joint with single microtrichia of *Eristalis tenax*; (E) multiple *microtrichia* on each micro-plate joined by flexible membrane *Eristalis tenax* on head-trunk membrane; (F) mixture of papillae-like and elongated microtrichia on neck-head membrane of *Myathropa florea*; (G) parallel microtrichia on microplates of side hip joint of *Eristalis tenax* [15].

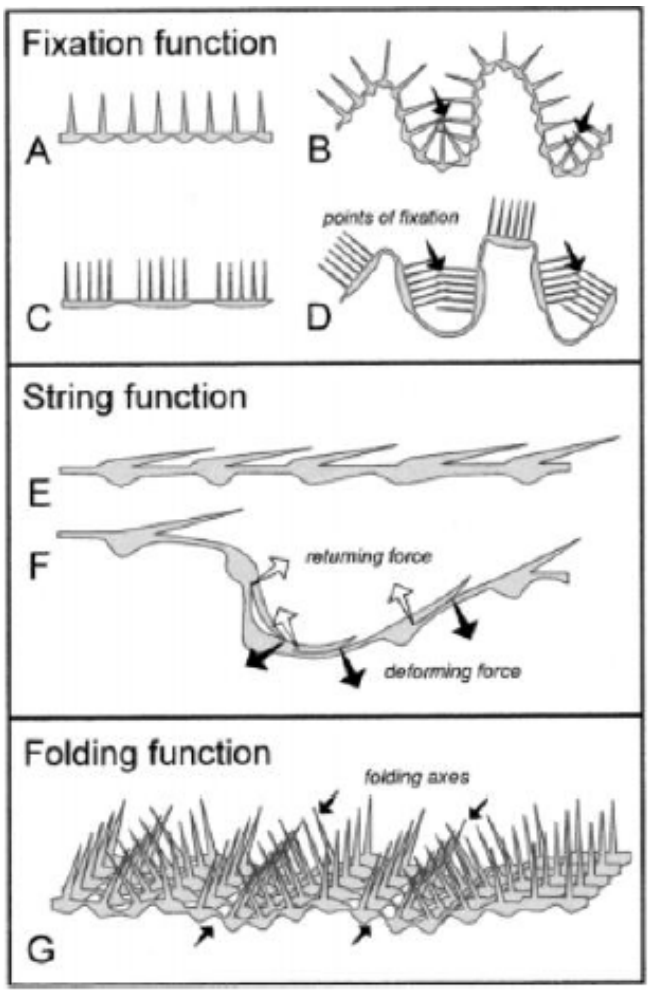

Figure 9: Possible functions of microstructure on membranous *cuticle* of various Diptera species. (A-D) Fixation function; (E-F) String function; (G) Folding function. [15]

As it can be seen in Figure 9 above, the functions are grouped into three categeories: fixation, string, and folding. Fixation allows for more stability. String function provides another degree of resilience to deformations in the membrane. And finally, the folding function allows for specific directions for the membrane to fold. With these differing microstructure, the *Diptera* species have the ability to control the function the membranous cuticle, which is key to investigating the mechanical performance of the various joints of the insect.

2.3 *Crack growth analysis of a composite/adhesive interface toughened by in-mold surface preparation* by Takuya Suzuki et. al. [11]

In this paper, the authors discuss the effect microstructures have on the interface toughness of a composite/adhesive material. They performed crack growth analysis using finite element method (ANSYS 12.0) to determine and investigate the effects of microstructure size and shape [11].

The most applicable information to the ant neck research came from the section discussing the microstructure of carbon-fiber-reinforced plastic (CFRP). They captured SEM images of the cross sectional view of the microstructure showing the wire-lines of carbon fiber, as seen in Figure 10A and B. This aided the strength and toughness of the composite/adhesive and decreased the chance of interfacial fracture.

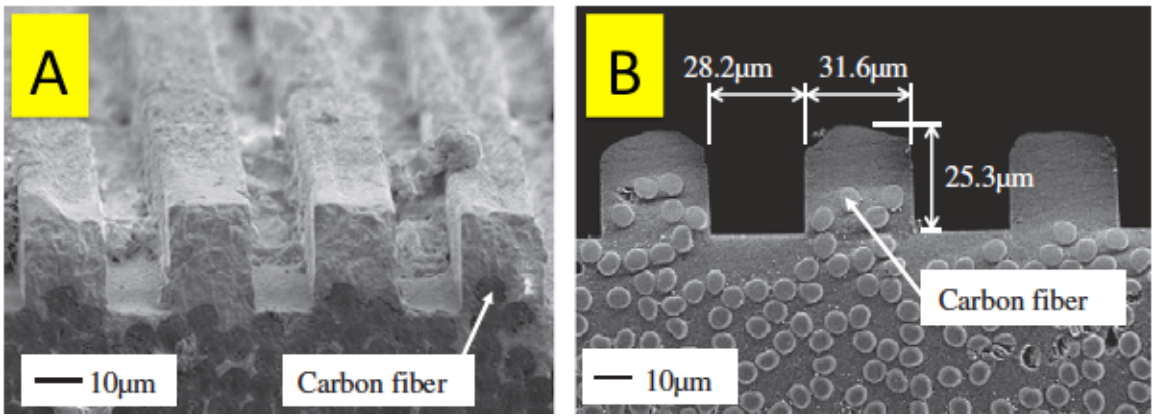

Figure 10: SEM image of CFRP with imprinted concave and convex structures. (A) Side view and (B) cross sectional view. [11]

The aspect ratio was also discussed, similar to what was done during the ant neck interface study under Owino. The amount of adhesive interface engagement seems to highly correlate with the type of rupture that occurs under loading. For

example in Figure 11A, there is a very low aspect ratio. This evenly distributed the crack growth across the teeth-like interface. The aspect ratio was then slowly increased, increasing the engagement area. The predicted interfacial fracture modes for these can also be seen in Figure 11.

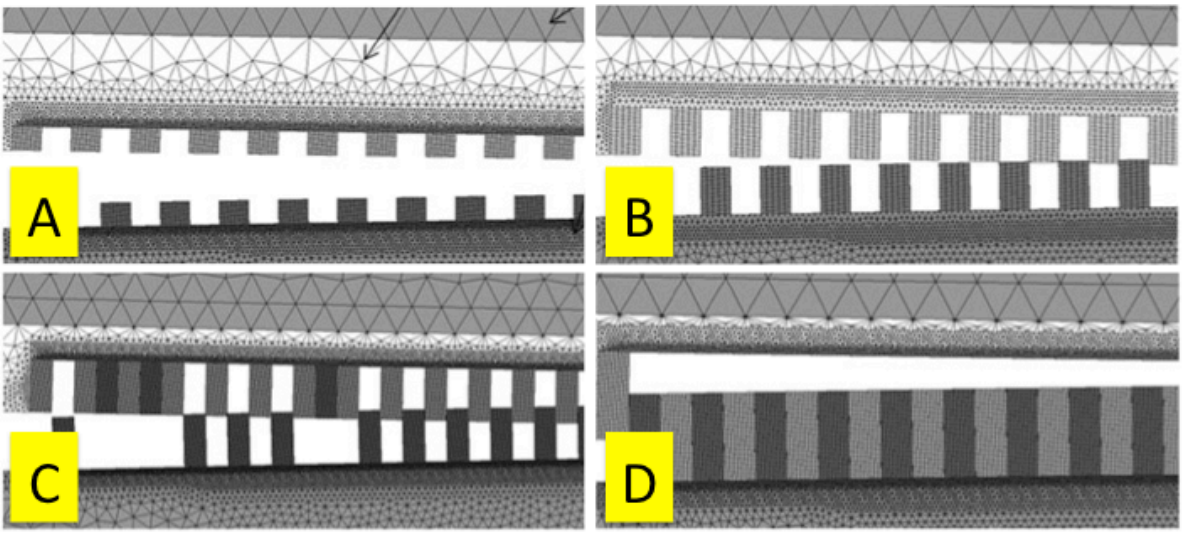

Figure 11: Fracture mode at the interface; interfacial fracture for a low aspect ratio and cohesive fracture for a high aspect ratio. (A) Lowest ratio to (D) Highest ratio [11]

This paper provided key ideas as to what to look for when analyzing the SEM images of the ant neck region. Though biomaterials will not have the carbon fiber reinforcements, they may have some other forms of fiber that may be traced. If the soft to hard transition in the neck membrane can be observed to be similar to the previous Figure 11 above, then it can be postulated that the carbon-reinforcement-like structure is what contributes to the strong adhesiveness of the neck membrane. This paper gave good direction as to what could possibly be found, despite one being a plastic composite and the other being organic biological material.

2.4 *Finite Element Analysis of an Adhesive Joint Using the Cohesive Zone Model and Surface Pattern Design of Bonding Surfaces* by M. J. Lee et.al. [12]

This paper discussed the technical and mathematical methods of analyzing various adhesive joints. The researchers utilized FEM to predict crack initiation, growth and even shape of fracture surface.

Similar to the finite element analysis done on the soft-hard interface in ABAQUS under Owino, this paper discusses the various "lap joints" that contribute to the rupture strength and characteristics. A single lap joint can be seen in Figure 12, which is very similar to the single-stepped interface analysis run under Owino, seen in Figure 13.

Figure 12: A single lap joint. [12]

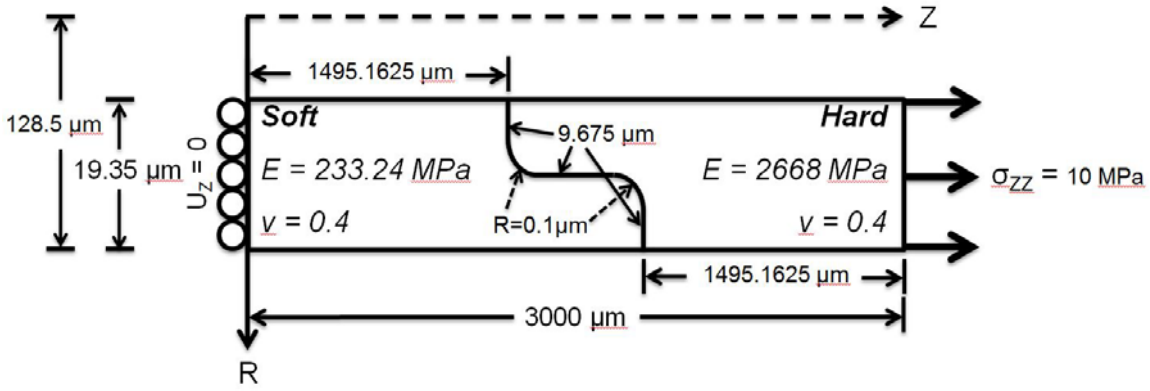

Figure 13: Axisymmetric model of the bi-material hollow cylinders with 1-step interface. [6]

Varying the pattern type and width changes the fracture surface under same loading. A cross section of the fracture surface for a single leg bending joint and an

end notched flexure joint can be seen run in Figure 14. Using these characteristics, the cohesive zone could be analyzed.

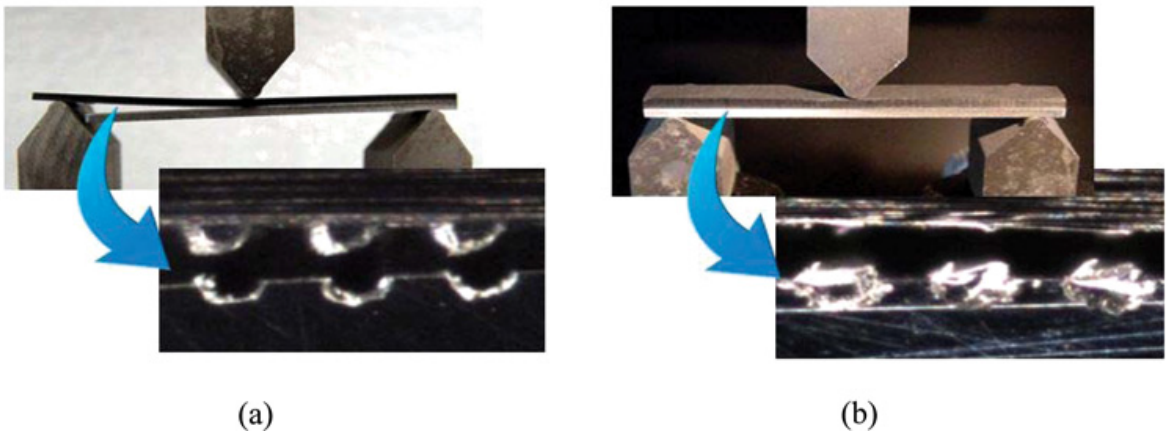

Figure 14: Cross section of the fracture surface for (a) the single leg bending joint, and (b) end notched flexure joint. [12]

2.5 *A Three-Dimensional Atlas of the Honeybee Neck* by Richard P. Berry et.al. [10]

This study reconstructed various 3-dimensional views of the Honeybee (foraging female bee *Apis mellifera*) neck generated from taking serial sections. This provided them with enough resolution to reconstruct any fine details of the neck region including the skeletal structures and even nerve branches. Unfortunately, all models are based on a single sample, due to the "laborious nature of reconstruction from serial sections"[10]. The high resolution of their model allows the ability to hide and show individual anatomical features such as individual muscles or nerves. This provided them with a good understanding of the head-neck region of the honeybee.

In order to recreate a 3D model, they took multiple images of each sectioned slice, and these images were stitched together creating a single high-resolution

image. They utilized various alignment methods to successfully stitch the images to render a clear final result. They used the software Amira 3.1 to create mesh models from stacks of segmented images, as seen in Figure 15.

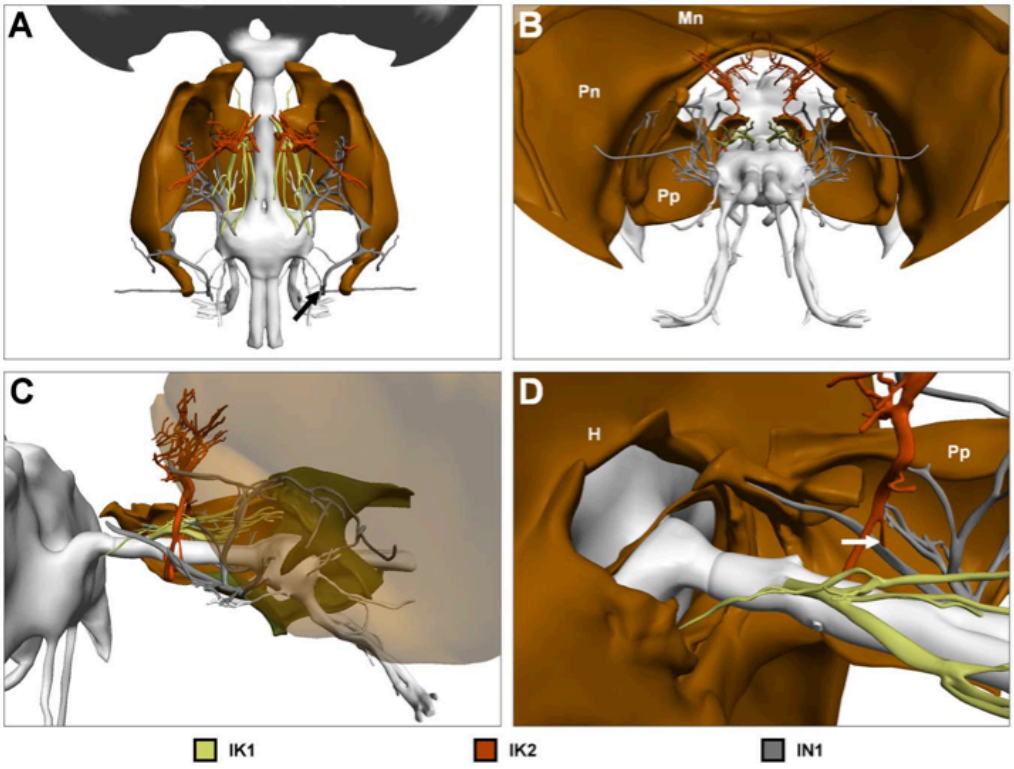

Figure 15: Ventral nerve cord (VNC) and nerves innervating the neck muscles. (A) Dorsal view of brain, VNC and nerves. (B) Posterodorsal view of nervous system with surrounding skeletal structures. (C) Lateral view (D) Enlarged view of nerve cord. [10]

A similar method was used in my study regarding embedding the actual specimen first before making the section cuts. In their method, they initially cut through the thorax and then submerging the head in fixative (3.7% formaldehyde, 2.5% glutaraldehyde in 0.01 M phosphate buffered saline). Small incisions were made in the eyes and thorax to aid in the fixing process. This allowed the fixative to completely penetrate the interior of the head. After letting these fix overnight,

further preparation was taken including embedding the specimen in Araldite 502/Epon 812 resin. They used microwave radiation and vacuum pressure to aid in the fixation process. These specimens were then sectioned using a diamond knife at 1μm intervals on a ultramicrotome. These serial section images were then imported into Amira for 3D model generation.

Despite this intricate methodology implemented in their study, they did not look into the microstructure of surfaces or interfaces throughout their research, which is of key interest for the ant neck project. However, this study still gave great inspiration for future studies. In future studies of the ant neck joint, similar steps could be taken once an ultramicrotome is made available for use in a local lab to capture images of thin cross sections of the neck. This will allow the recreation of a 3D model for various analysis including stress concentrations and rupture/fracture regions. This could aid in clearly defining the soft to hard tissue interface in the neck membrane, to provide further insight to reverse engineering the adhesive qualities of this region.

Chapter 3. Methodology

Initial ideas for retrieving the desired cross-sectional cut included the use of scalpels, sanded down paper clips, dental picks, razor blade, and Exacto-knife. The best attempts at dissecting the ant neck region were made using the Exacto-knife. For the remainder of this paper, this method will be referred to as Method 1. Method 1 was a useful technique to get the general idea of the geometries and images of the ant neck region, but often failed in cutting a clean cross section. Many dissection attempts ended in tearing large masses of the neck region instead of actual clean slicing.

Since Method 1 did not provide the desired resolution, we devised an improved method consisting of embedding the entire ant in acrylic resin, allowing it to solidify completely, then using a milling machine and a fine end mill to mill the desired ant neck cross section. This approach, referred to as Method 2, gave excellent control of cross-sectional cuts. This chapter focuses mainly on the methodology followed for Method 2.

3.1 Obtainment of Specimen

In order to obtain ant specimen, George Keeney at OSU Aronoff Greenhouse / Insectary was contacted. At the insectary, there are various species of insects available for entomological research. Care must be taken before arriving at the site, such as no open-toed shoes, in case any dangerous insects escape. Most species available at the insectary are harmless, but they do house some poisonous species,

such as the Vietnamese Millipede and Venezuelan Suntiger, pictured in Figure 16A and B.

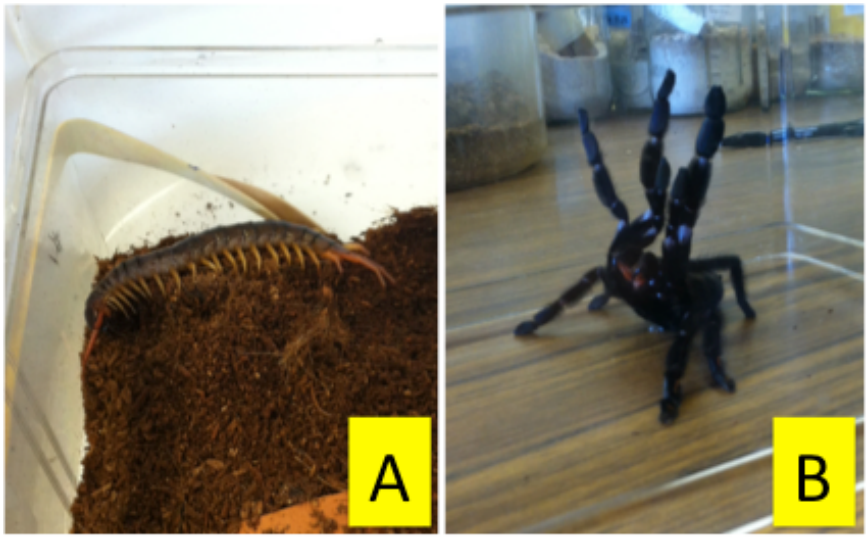

Figure 16: Both photographs taken at OSU Insectary. (A) Vietnamese Millipede. (B) Venezuelan Suntiger at its intimidated stance.

For the initial specimen obtainment for this particular research in Summer 2013, *Formica exsectoides,* also known as Allegheny Mound Ants were available for pick up. Approximately 20~30 ants were picked out and placed into a transportable container. The top one-inch of the container was lined with painted Insecti-slip (Fluon, PTFE coating) to prevent the ants from escaping out the top when the lid was removed. The colony did not include a queen ant, but solely consisted of worker ants. Without the queen, Keeney estimated that the colony would survive approximately one to one and a half months.

3.2 Care of Colony

The ants were kept in a dark room at room temperature (approximately 70 degrees Fahrenheit) with the lid placed tightly on to prevent any escape. The container set up consisted of two glass test tubes, water, cotton balls, tin foil, sugar cubes and honey water (1:1 ratio for honey and water). The test tubes were filled with water half way, and two cotton balls stuffed to prevent the water from escaping. The tin foil was used to wrap the opening of the test tubes to keep the "dry" area inside the test tube damp with high humidity for the ants. The tin foil had a hole large enough to allow ants to crawl in and out of the test tubes, creating a housing for the colony. These test tubes were placed horizontally in the container with model clay at the ends to prevent them from rolling. Dry sugar cubes were placed in a separate location in the container next to some honey water. This set up provided enough water and food supply for the entire colony for several weeks. An example of this set up can be seen in Figure 17 below.

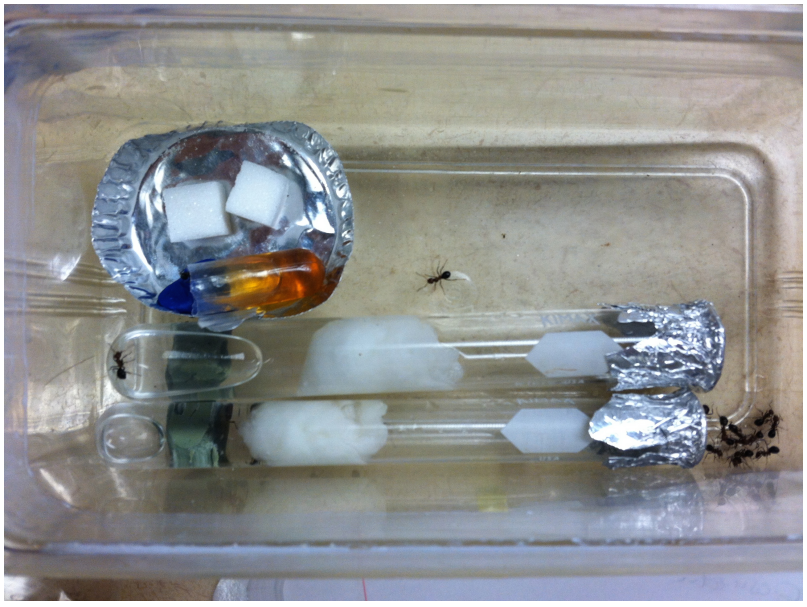

Figure 17: Photograph of ant colony care setup.

3.3 Preparation of Specimen

The initial stages for preparation of specimen followed Nguyen's protocol for SEM imaging. First, the specimens were placed in a killing tube or jar with ethyl acetate. The fumes of the chemical were enough to quickly kill the ants. The specimens were then cleaned using ethanol 70% in a separate Eppendorf tube. This process washes any extraneous dirt off of the ant body for cleaner images in imaging machine. After cleaning the samples, they were placed on a petri dish with the lid taken off and then placed under a fume hood to dry 2~3 hours or overnight.

Once the samples have been thoroughly dried under the fume hood, refer to the protocol in Appendix A for embedding ants in acrylic resin for detailed methodology on how this was prepared. The completed samples can be seen in Figure 18, successfully cast in hardened acrylic resin. Figure 18A is a photograph of a side view of the hardened acrylic with one single ant specimen embedded in it. B shows the view from the top of the opening of the Eppendorf tube. C is the collection of embedded samples.

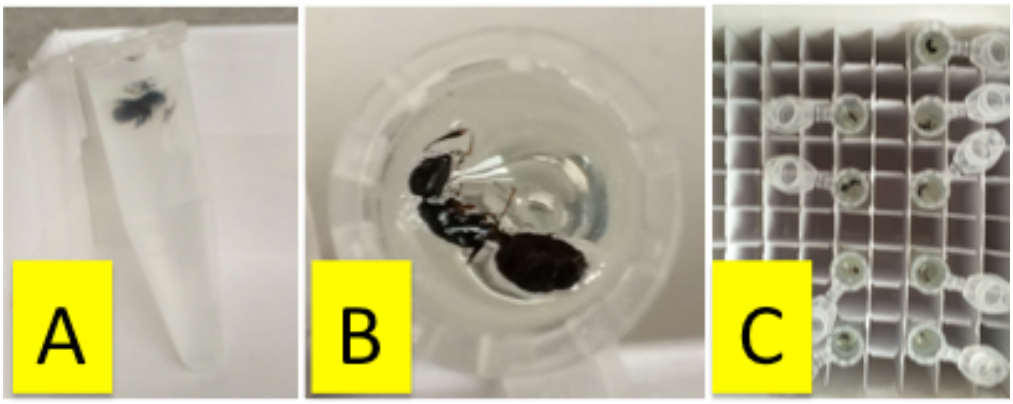

Figure 18: (A) Side - (B) Top - view of specimen embedded in hardened acrylic resin. (C) Samples stored in batches for further analysis.

3.4 Dissection Using Milling Machine

As previously stated, Method 1 did not offer a precise cross sectional cut of the ant neck region. Utilizing an Exacto-knife razor as the primary tool for cutting did not allow for any angle or location specifications. The milling machine with a very fine end mill was a possible alternative to consider, as Method 2.

In order to work with such small organic materials, a super fine end mill was specially ordered, as the student machine shop did not carry appropriate sizes for these incisions. Throughout the process, 1/8”, 1/16”, 1/32”, and 1/64” sized square end mills were used for various cuts. A photograph in Figure 19 gives a size comparison of the end mills. The smallest end mill in the red holder is the 1/64” end mill.

Figure 19: Photographic comparison of 1.5 mL Eppendorf tube with embedded ant in acrylic with 1/64", 1/32", 1/16" end mills (from left to right).

The motor speed was run at the machine’s highest capable and safe speed at around 3300 RPM on the Seiki VS Vertical Mill, as shown in Figure 20. Figure 21A

shows the set up of the embedded specimen held firmly in the vice, ready to be milled. B shows the final result after taking multiple section cuts, as outlined in detail in the protocol section in Appendix B for machining ants. C shows the top sectioned surface of the Eppendorf tube, drawing particular attention to the fact that desired angles can be cut using this method. The most difficult step was nearing the actual neck region of the ant, as the ant still has the capability to fly out of the embedded acrylic if the tool happens to grab the organic tissue of the ant. It was important to take as little off at a time in this region, no more than 3 thousandth of an inch (thou) per pass, with a slow but steady feed-rate. A light and scope was used to check neck exposure after each pass, to determine if further passes were required.

Figure 20: Speed for this particular milling machine was at approximately 3300 RPM (in the red zone) on High.

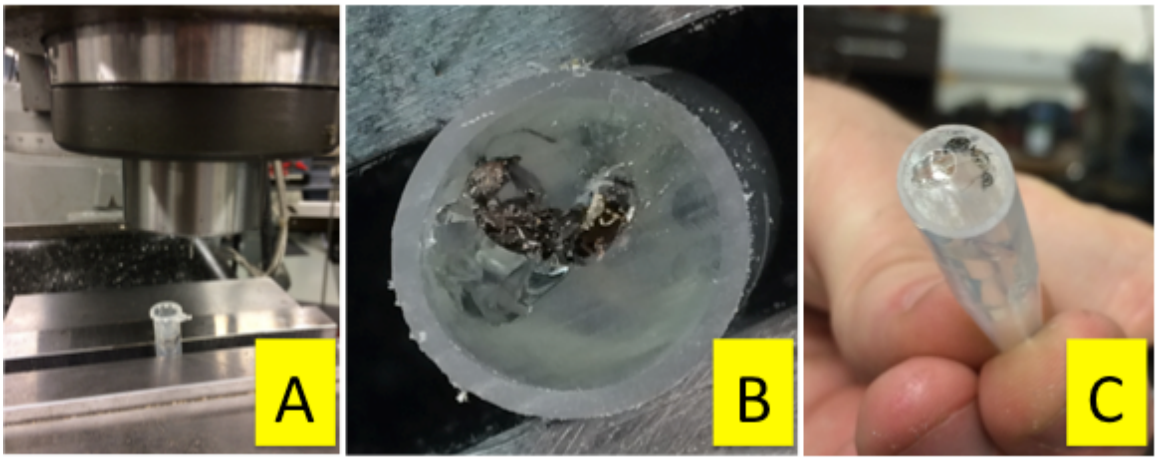

Figure 21: (A) Embedded specimen in Eppendorf tube firmly gripped at desired angle using vice. (B) Desired cross-section achieved after multiple careful passes. (C) Top surface view of cross-sectional cut.

3.5 Imaging with Standard Light Microscope

Before taking the sectioned neck samples to CEMAS for sputter coating and SEM imaging, some were imaged using the standard EVOS light microscope in the Nanoengineering and Biodesign wet lab, as seen in Figure 22A. Figure 22B shows an example image captured using this method. Although this method did not provide high-resolution images for the surface microstructure, it provided good feedback on which samples would be good to image. This method acted as a secondary check to see if the desired cross section was indeed made. In some cases, it was found that the end mill did not in fact go through the acrylic into the neck membrane and these samples could be machined further.

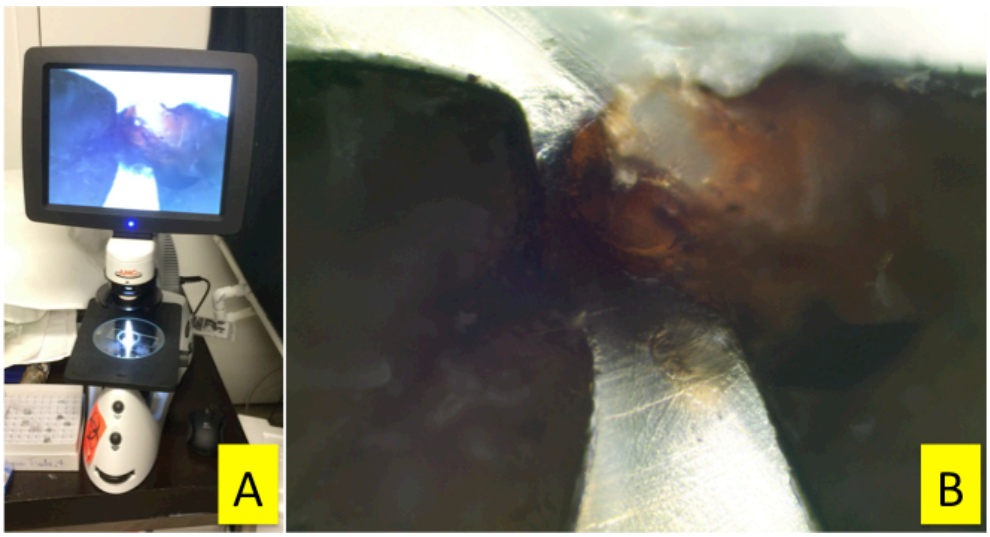

Figure 22: (A) EVOS standard light microscope set up. (B) Corresponding sample image of ant neck cross section (side view, head to the left, body to the right) taken on the light microscope.

3.6 Sputter Coating at CEMAS

Once the desired cross-section had been cut using Method 2, the samples were taken to CEMAS for sputter coating. The detailed instructions on using the sputter coating machine can be viewed in Appendix C under the sputter coating protocol. Once the samples were sputter coated, colloidal graphite was used to make the connection between the top coated surface and the sides of the acrylic, as the coating process only coats the top horizontal surface and not the sides. These were then placed in a drying oven at 50 degrees Celsius, also located in CEMAS lab. The samples were left in the oven for approximately 10 minutes. These steps can be seen in Figure 23.

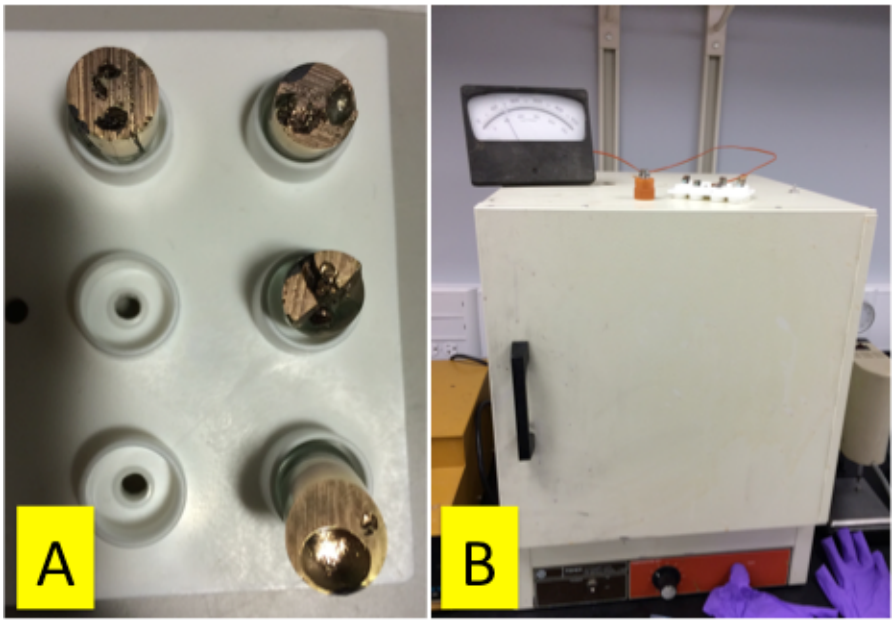

Figure 23: (A) Samples sputter coated and streaked with colloidal graphite. (B) Drying oven at CEMAS set to 50 deg C.

3.7 Quanta 200 SEM Imaging

Scheduling a time slot for SEM imaging on the Quanta 200 must be done well in advance. This can easily be done through their new online system called Facility Online Manager (FOM). For first time users of any particular machine, a training session with Cameron Begg or a facility manager must be scheduled. Various procedures and techniques are taught during this half-hour to an hour training session. After the completion of the training session, the user now has access to FOM for future scheduling. Detailed guidelines are outlined in the protocol section in Appendix D under Tips for Quanta 200 SEM.

The biggest difference between imaging the initial samples using Method 1 and final samples using Method 2 was the difference in stage mounts in the Quanta 200. For the sections made using Method 1, the samples were loaded onto

Aluminum SEM pin studs, then sputter coated. For these samples the standard default SEM pin stud mount was used to grip the samples. For Method 2 using the acrylic, a new vice had to be mounted to firmly grab the sample, as it can be seen in Figure 24. This spring loaded diamond-shaped vice allowed for easy placement and removal of the specimen.

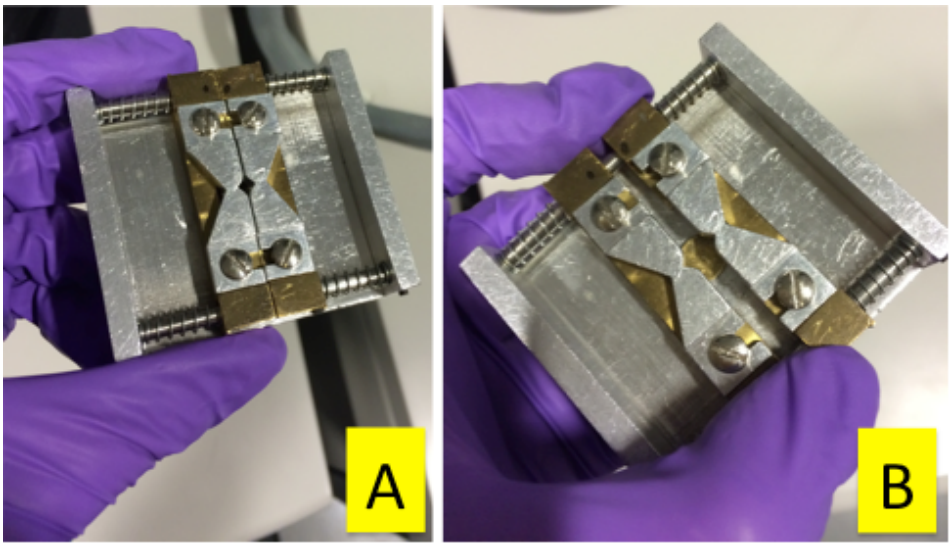

Figure 24: (A) Spring-loaded vice for use in the Quanta 200 SEM for Method 2 in the closed position. (B) Vice in the open position for sample placement.

Once the sample is loaded into the SEM, the door is shut and the machine pumps out air in the chamber, creating a near ideal vacuum for image capture. The samples must be conductive in order for any images to appear in the image analysis computer, which explains the importance of using colloidal graphite for tall single standing samples such as ants embedded in acrylic. Figure 25 shows the general station set up for the Quanta 200 at CEMAS, where images can be captured, recorded, and saved on the image analysis computer while the samples are sitting in the SEM chamber.

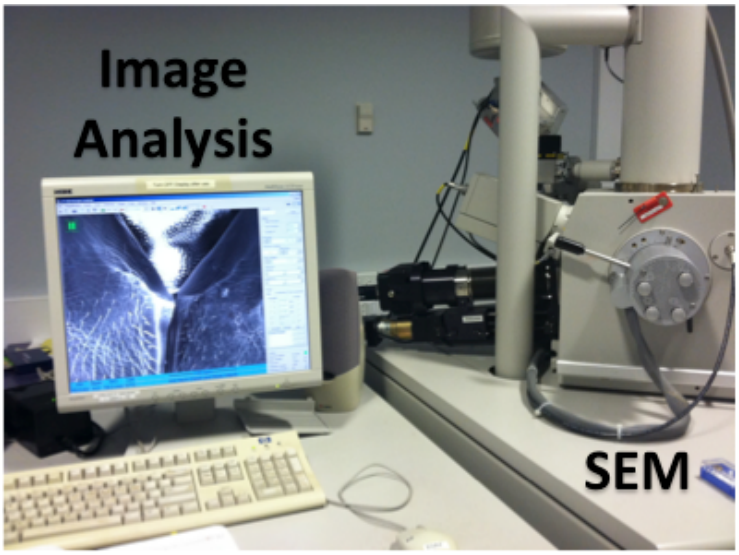

Figure 25: Quanta 200 table set up with the image analysis computer to the left and the SEM chamber equipped with high speed, high-resolution cameras to the right.

Once the sample is set in vacuum, the user can use the computer to image, capture, and analyze the specimen on the screen. There are various functions in the program including: zoom (+/-), image refresher speed (turtle/hare), focus, contrast, brightness, and various others. The general imaging process includes: (1) initial image capture of entire specimen surface to gain an overview perspective, (2) zoom in gradually to desired location, (3) utilize focus and contrast as needed before each image capture, (4) re-label the image title for future reference, (5) freeze the image using the camera button and (6) save the file onto designated folder. These images can be accessed online at [data.cemas.us] with updated credentials.

Chapter 4. Results - Scanning Electron Microscopy (SEM) Images

As described previously, Method 1 did not yield clear cross sectional views of the ant neck joint when placed in the SEM machine for imaging. However, upon improvement of the dissection and preparation method to Method 2, a clear transition point between the soft and harder material was discovered.

4.1 Initial SEM Images

Method 1 yielded several good cross sectional images, despite the difficulty in getting a clean dissection. The image below in Figure 26 shows a sagittal view of the right half of a *Formica exsectoides* (Allegheny Mound ant)'s head and neck. The rest of the body was excess material and was removed for imaging.

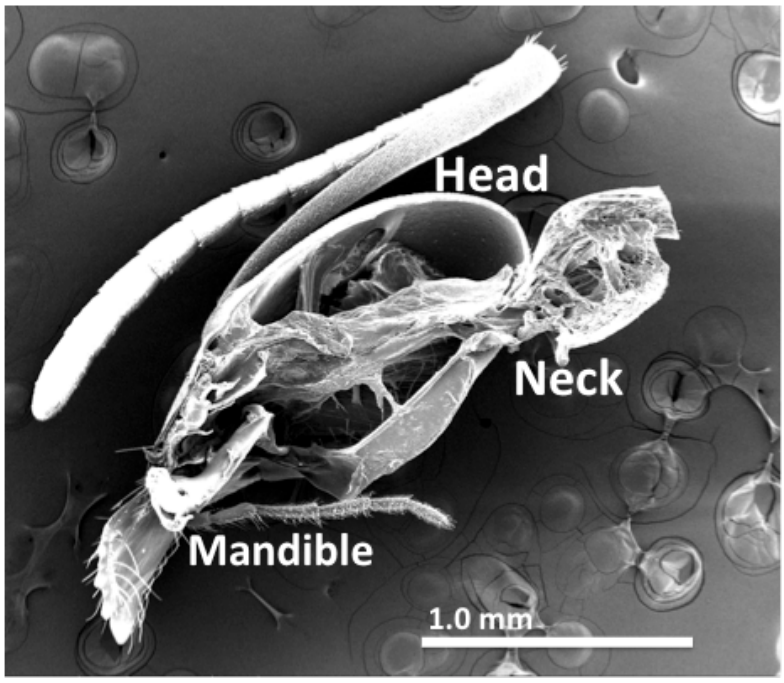

Figure 26: SEM image of sagittal view of *Formica exsectoides* head and neck.

Multiple attempts were made to dissect the neck region in such a way to successfully expose the neck region to study the soft-hard interface of the neck membrane. In Figure 27A and B, an interesting observation can be made in the neck to head region. Even though the desired section was not cut due to the imprecision of the method, this image reveals that there are fiber/string-like material that extend out from the neck region attaching to various locations on the interior of the ant head. This could potentially contribute to the incredible tensile strength of the neck membrane, similar to previously discussed CFRP with the reinforcements. A different perspective of this can also be observed in Figure 28 seeing from the under-side of the head-neck region.

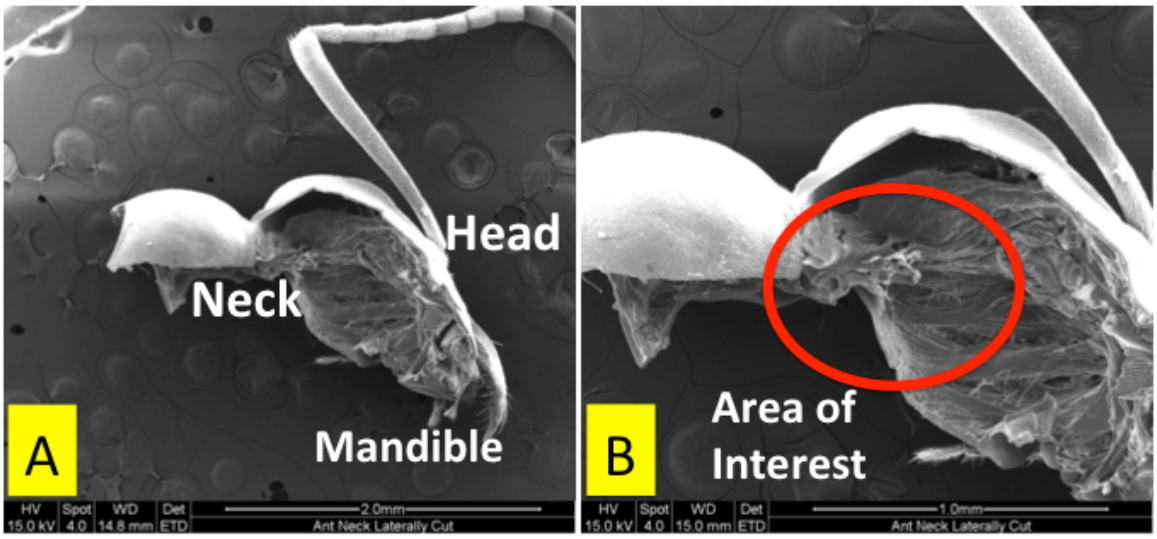

Figure 27: SEM image of left half of *Formica exsectoides* head and neck. (A) Overview of image. (B) Close-up view of and neck region.

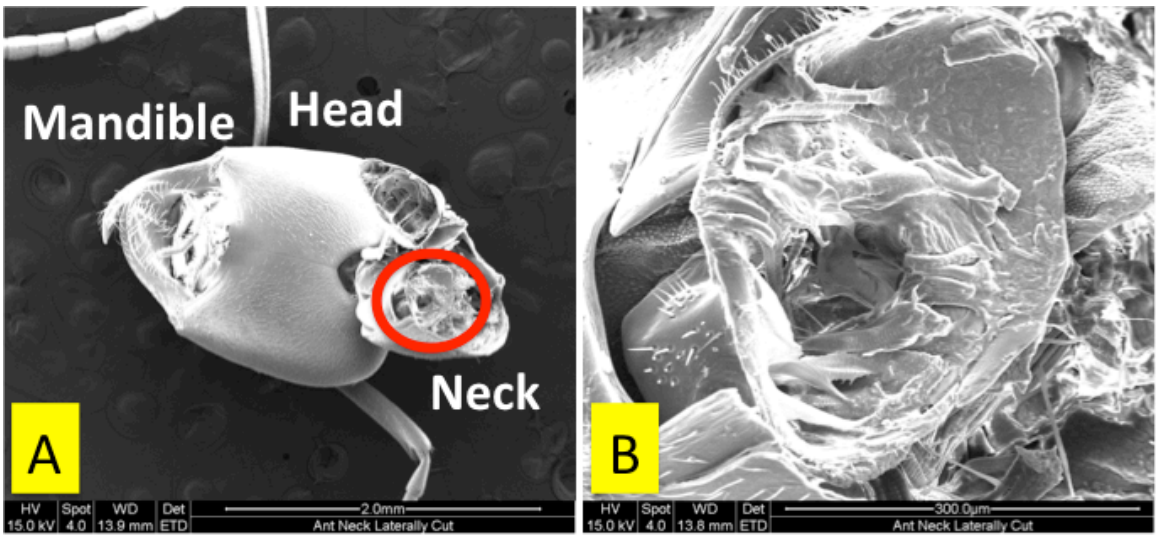

Figure 28: (A) View of under-side of the head. (B) Close-up view of red region in A, showing the reinforcement-like structures that connect the head to the body through the neck region.

Using an Exacto-knife did not provide the precise incisions as desired, but still provided some great SEM images such as Figure 29 below, where the ruptured and torn head region can be seen with the soft neck region exposed. The collarbone like structure is the exoskeleton chest plate of the ant body surrounding the neck joint. Figure 30 shows the back of the head that was torn off of the body, which allowed for closer imaging of the head-neck region.

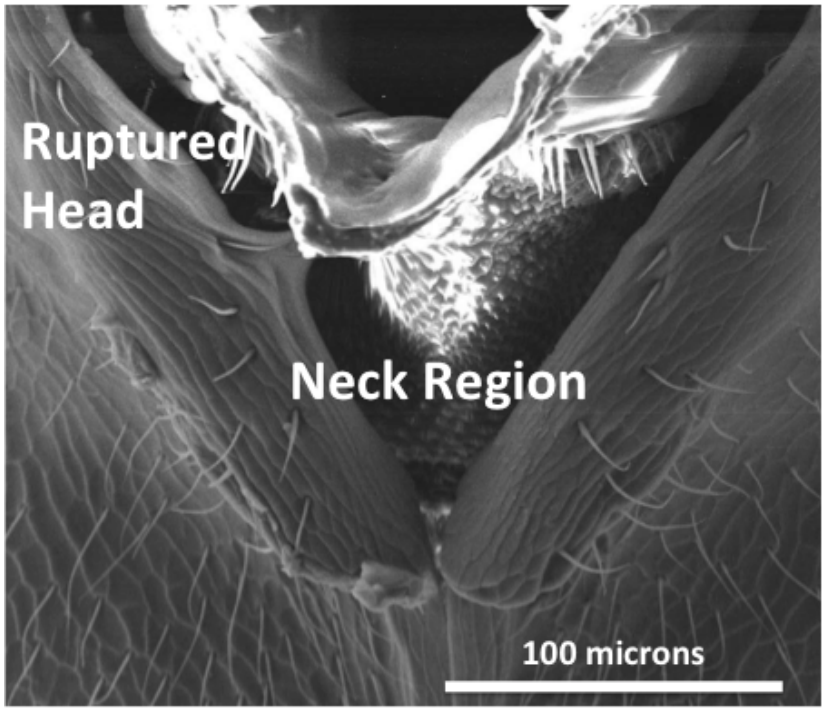

Figure 29: SEM image of ruptured head with collarbone like structure surrounding soft neck membrane.

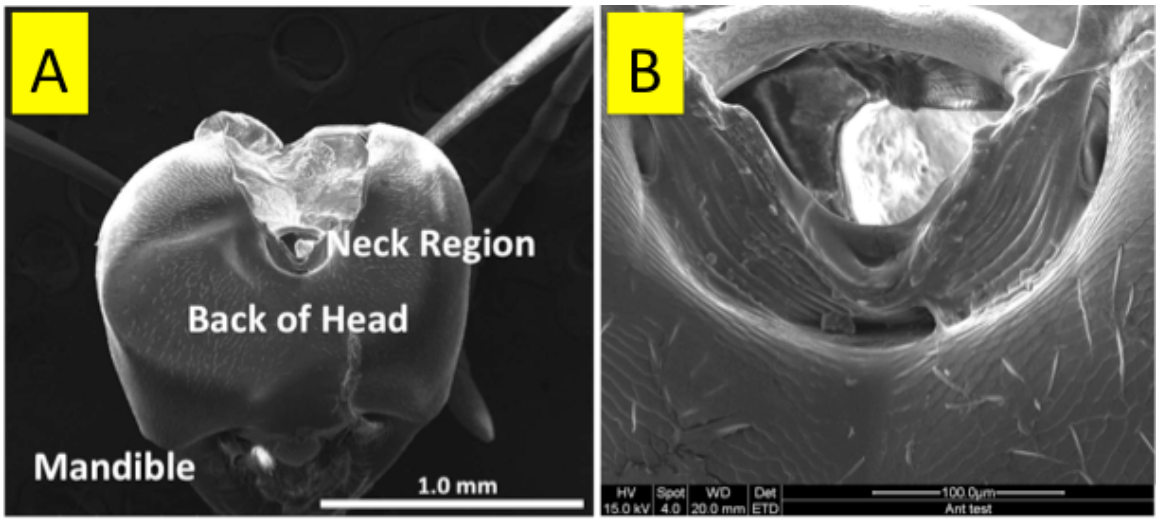

Figure 30: SEM image of back of ant head. (A) Overview (B) Close-up view of neck region.

In general, though the method yielded good images, the dissection method needed to be improved to get desired angles and better resolution cross-sections.

4.2 SEM Images Using Improved Methodology

Method 2 consisted of embedding the ant specimen in acrylic and milling the desired cross-section using a milling machine and fine end mills. This method allowed for more precise angle of sections and provided a stable fixture for the cutting cool. This improved technique allowed the specimen to be statically gripped while the desired incisions were made.

With the new spring-loaded vice to grip the acrylic, the samples were similarly imaged using the Quanta 200 SEM, as seen in Figure 31. This image taken at CEMAS shows the spring loaded diamond-shaped vice making contact with the black colloidal graphite, creating the conductive connection to successfully generate the clear SEM image.

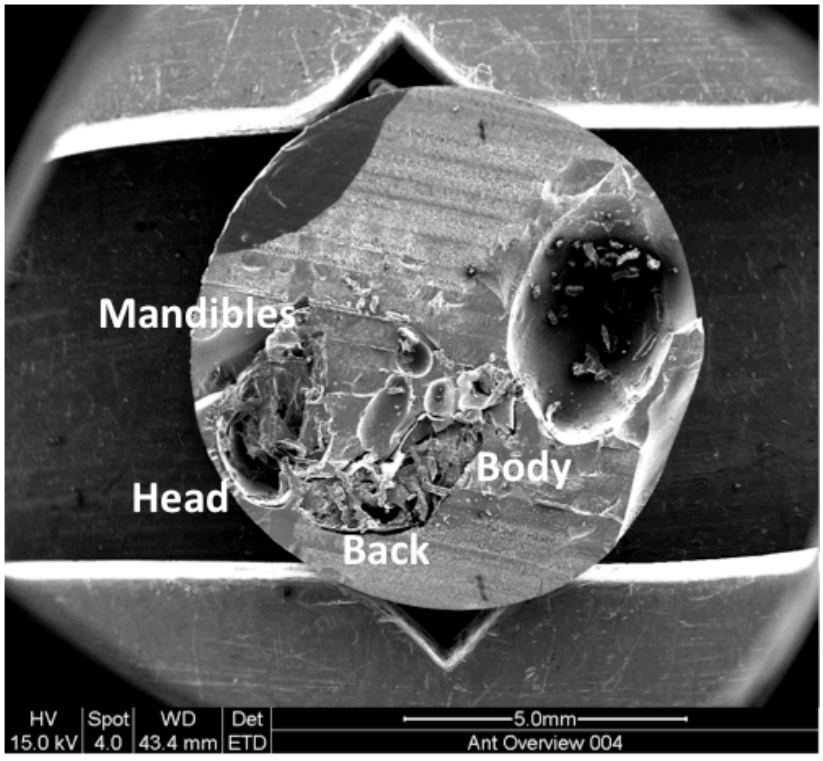

Figure 31: SEM image of carpenter ant embedded in hardened acrylic resin. This is the sagittal view showing the left half of the ant.

Initial attempts using Method 2 proved that a slower feed rate and smaller end mills were required. In Figure 32A below, it can be seen that the cross-section was indeed made through the acrylic, but due to the fast feed rate and large end mill utilized, the actual soft tissue membrane was twisted backward into the body of the ant. Figure 32B, the close up image of the red outlined region in A shows the surface texture of the soft tissue membrane.

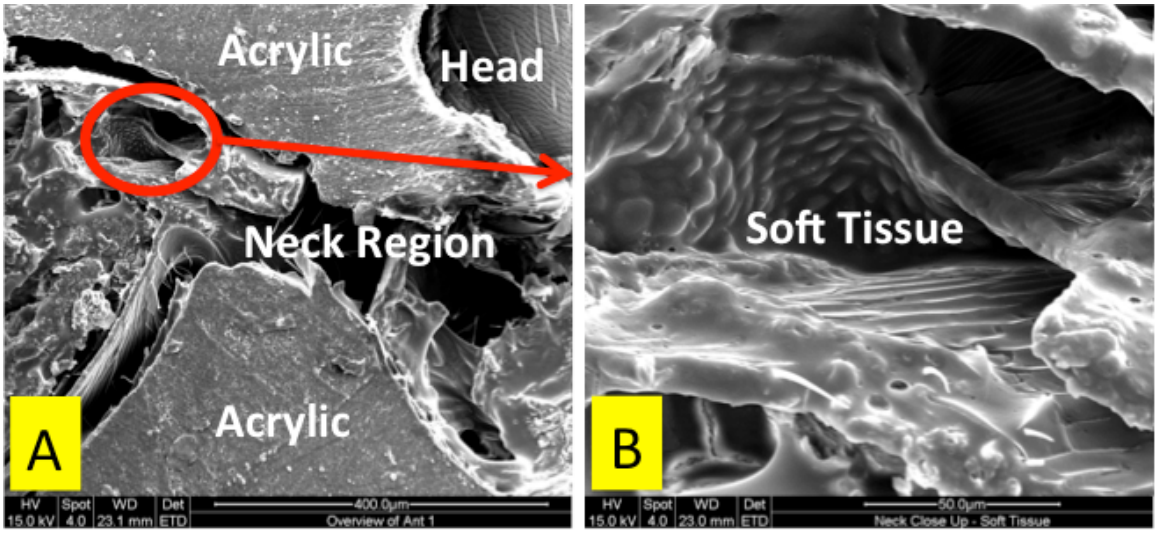

Figure 32: SEM image of carpenter ant neck region cast in acrylic resin. (A) Overview (B) Close up of red circular region in A that shows the soft tissue area of the neck membrane.

During the different machining and imaging stages of the study, it was found that timing was important in retrieving accurate, high-resolution images of the ant neck region. The usual routine consisted of having the cross-section machined and the desired neck membrane exposed one day, then waiting no more than one week to have the specimen sputter coated. This resulted in the soft neck membrane showing images such as in Figure 33A. However, if more than one week goes by before sputter coating the sample after dissection, the soft neck membrane dries up,

as if the fluid in the pockets emptied out, as seen in Figure 33B. This contributed further to the understanding of the neck joint, that for the carpenter worker ants, these soft tissues in the neck membrane uses fluid to assist in elastic movements of the neck.

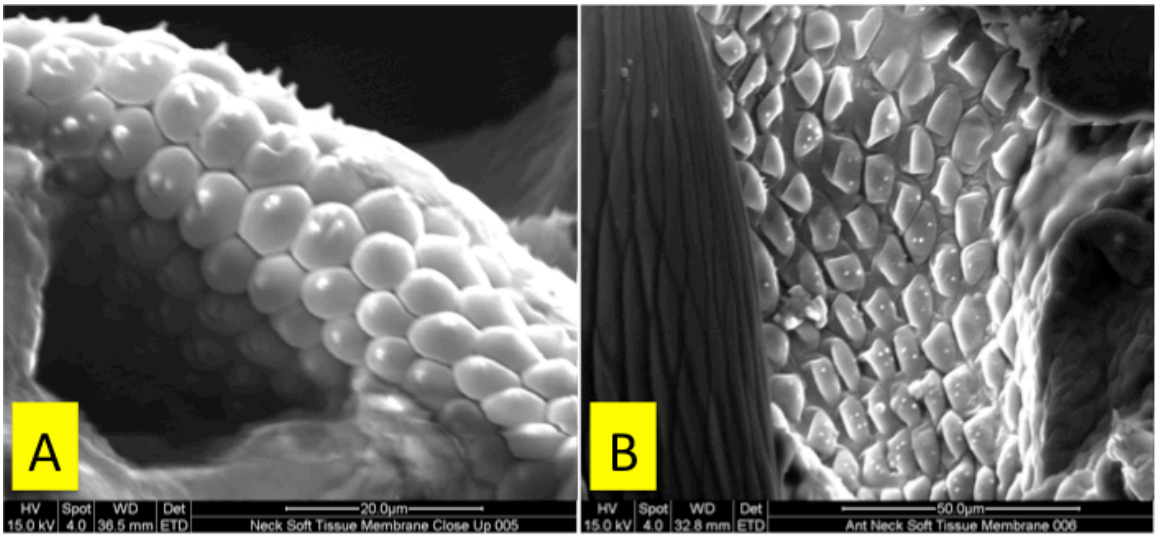

Figure 33: (A) SEM image of normal soft tissue region with fluid filled pockets. (B) SEM image of soft tissue region after fluid had escaped the pockets.

The same specimen from Figure 33B above was imaged in a different region of the neck and an interesting discovery was made in the image that follows in Figure 34. Even though the soft fluid membrane of the neck dried out and became brittle, the acrylic wall acted as a mold for the casting and retained the original bubble-like shape. If desired, this could potentially used to recast the soft tissue of the carpenter neck membrane and to study more in-depth the patterns of these fluid-filled pockets that allow for elastic movement. Figure 35 displays this soft membrane region, spread throughout the underside of the ant neck region.

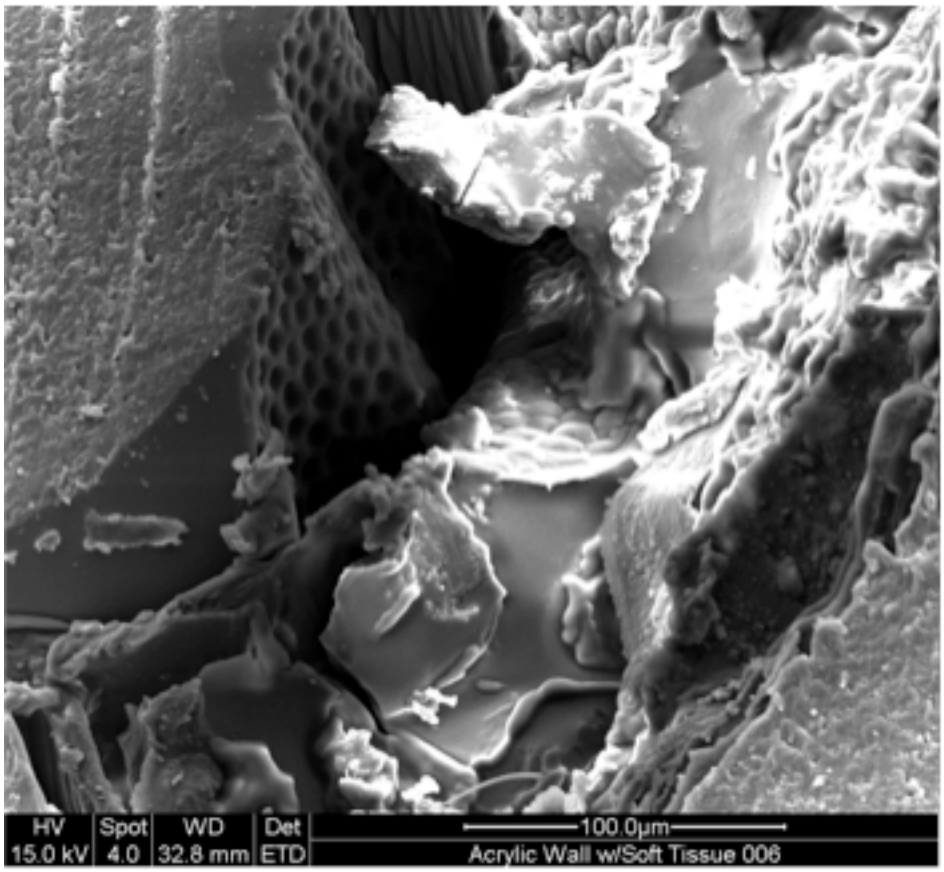

Figure 34: Acrylic wall that retained the original shape of the soft tissue fluid pockets similar to a mold.

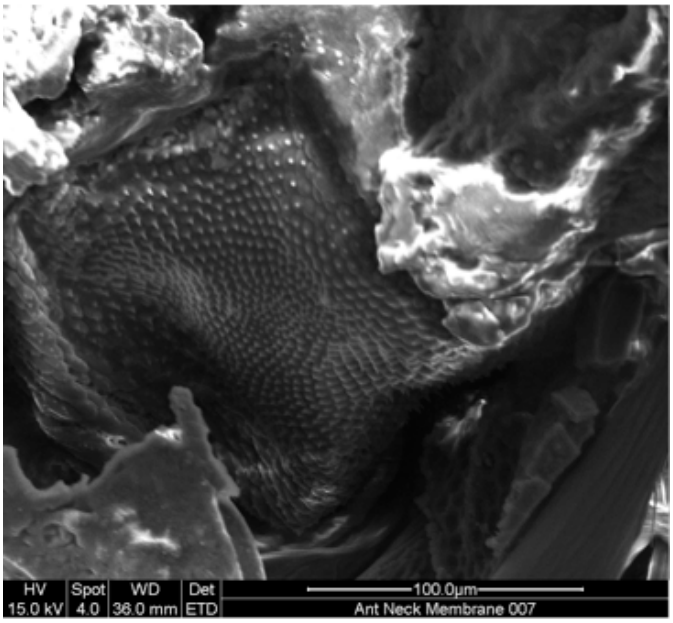

Figure 35: SEM of soft tissue membrane in the neck region of carpenter ant.

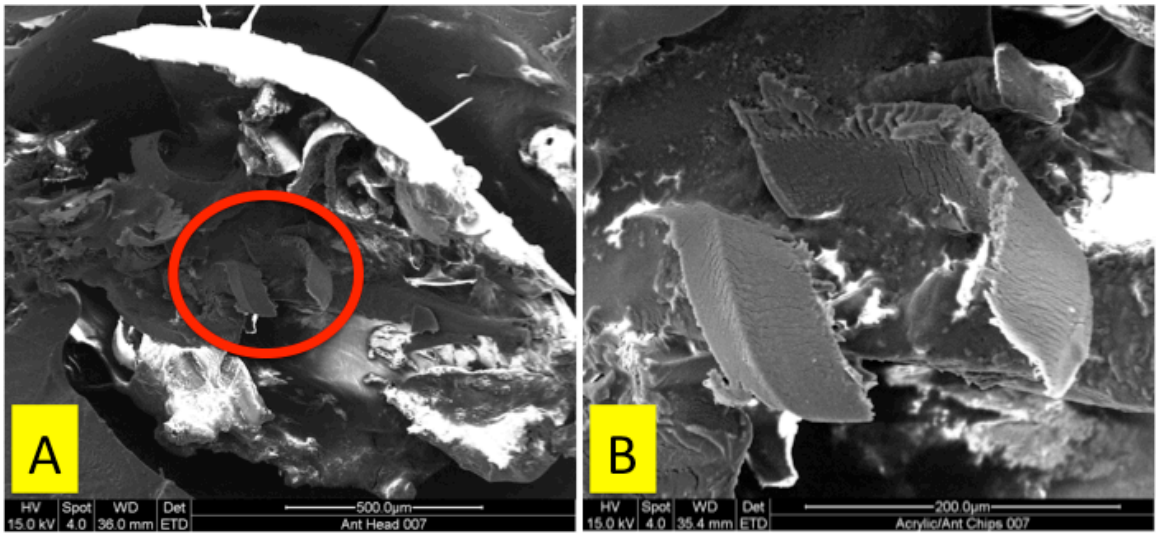

Figure 36: (A) SEM image of left over acrylic chips from 1/64" end mill. (B) Zooming into red circular region in A, the acrylic shavings can be seen.

Figure 36A and B above shows the importance of clearing off the chips at the machine shop after the desired cross section is cut. An air hose can be carefully used to blow off these acrylic shavings to avoid interfering with the imaging process. These images did however give a good indication of the size of the end mill flutes in comparison to the head-neck region of the carpenter ant. These shavings are most likely from the 1/64" end mill as the final tool used to achieve this cross section. It also illustrates the number of passes the process takes in order to achieve the desired cross section. These were no more than 3 thou passes on the milling machine, especially nearing the neck joint region.

Coming to the final discovery of the transition point, Figure 37 below gives an overview of the set up of the SEM image. The carpenter ant, cast in acrylic was machined using varying sized end mills. The end mill cuts can actually be seen in the acrylic upon close inspection of the image.

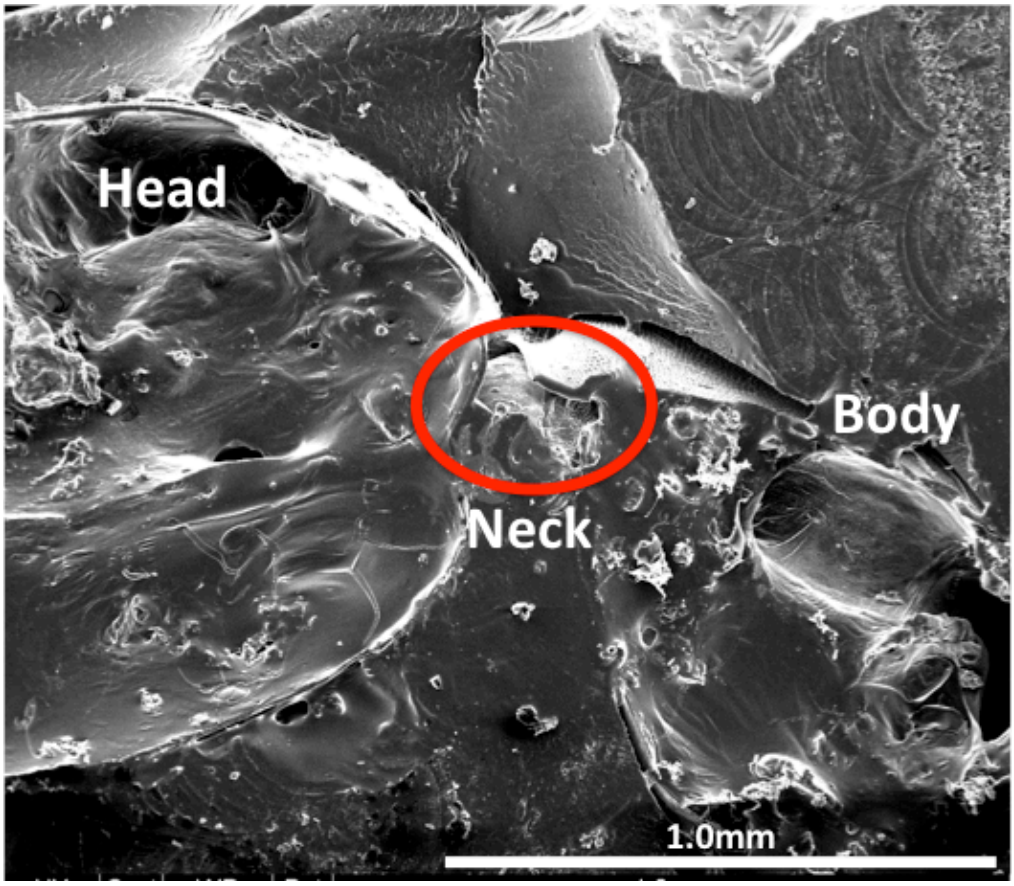

Figure 37: An overview of the SEM image exposing the exact desired neck region.

The anticipated transition point can be seen zoomed into the red circular region in Figure 37 above, seen in Figure 38A and B below. The transition takes place from soft to harder material, right to left. The fluid filled pockets that make up the soft membrane of the carpenter ant seem to elongate at various locations and transform into a newer most likely harder material. This is the soft-hard surface microstructure of this particular ant neck membrane that gradually extends the soft tissue into the harder material that eventually connects to the exoskeleton of the head.

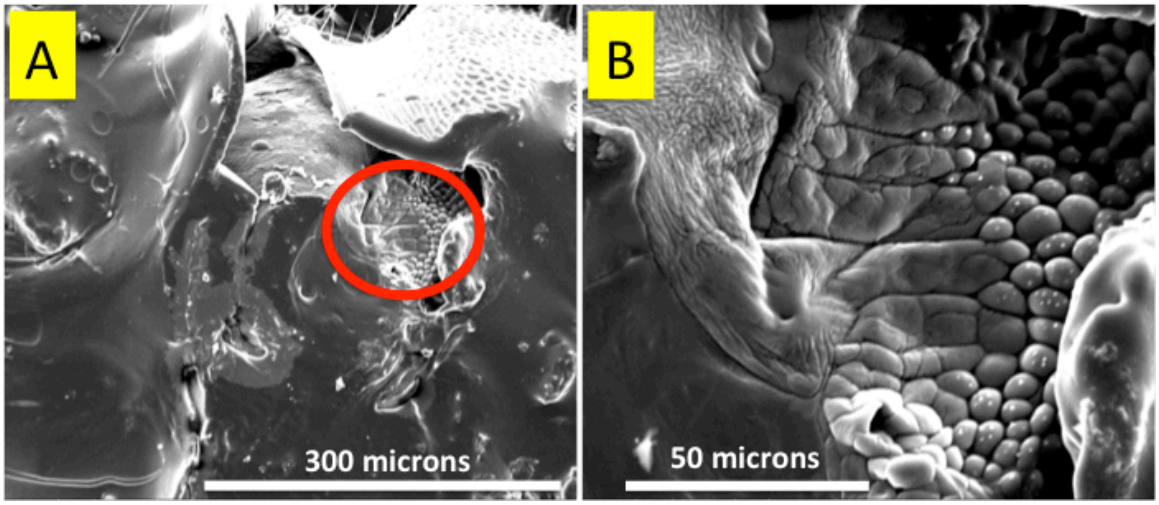

Figure 38: (A) SEM image of zoomed in view of Figure 37. (B) Close up view of the transition point showing the surface microstructure change from soft to harder tissue.

This discovery on the carpenter ants can be set as the basis for future comparisons of surface microstructure of the neck region of different species of ants. The soft-hard interface can be imaged and compared across different types of ants as well as even among same colonies (queen, worker, etc) to aid in the further understanding of the ant neck structure that gives the insect such incredible tensile loading capabilities.

Chapter 5. Conclusion

The most important contribution of this study was that it developed a successful process that future researchers may follow to retrieve similar SEM images across different species to be able to compare and contrast the surface microstructure. Though only carpenter ants were available for imaging using Method 2 during this study, different species can be embedded in acrylic, machined and imaged using similar methods. In this manner, species that are capable of high tensile loading such as *Formica exsectoides* can also be imaged using Method 2 to compare the microstructure against the carpenter ants (non-high tensile load bearing).

Through imaging, we were able to determine a clear transition point from soft to harder tissue in the neck region. This will be set as the basis for future comparisons across different species. These improved resolution images of the material, surface and interface microstructure will aid in the further understanding of the mechanical function of the ant neck joint.

In addition, Method 2 could be further improved by changing the approach of sample preparation. There are possibilities of utilizing wax as the medium for embedding specimen in order to take thin sections of the ant neck region using paraffin wax slicers as used in the medical field. These devices are often used to slice thin tissue samples to image desired cross-sections. This method would potentially allow for more accurate images of the surface microstructure at the neck joint. With

multiple thin layers available, these cross-sections could be first imaged using the standard light microscope, then possibly in the Quanta 200.

Future work will include collaboration with Dr. Sandra Metzler and graduate student Akul Kakumani on designing and building a linear micron stage for mechanical testing. The new testing stage design will give good control of the loading angle on the neck (load up, down, left, right) as well as provide better resolution imaging. Further information can be found on NSF Project Description for the study of the ant neck joint submitted under Dr. Carlos Castro (PI).

References

[1] Wojtusiak, J., E.J. Godzinska, and A. Dejean. "Capture and Retrieval of Very Large Prey by Workers of the African Weaver Ant." *Tropical Zoology*, vol. 8, no. 2, pp. 309-318, 1995

[2] Hoyland, S., *Nest Construction by O. Smaragdina Workers.*

[3] Castro, C., Katsube, N., and Lilly, B. "Reverse Engineering the Functional Design of the Ant Neck Joint." *IOS Preliminary Proposal.* (2013)

[4] Nguyen, V., Lilly, B., and Castro, C. "The Exoskeletal Structure and Tensile Loading Behavior of an Ant Neck Joint." *The Journal of Experimental Biology* (2012)

[5] Ichikawa, Kohei, Yuichiro Shin, and Toshiyuki Sawa. "A Three-Dimensional Finite-Element Stress Analysis and Strength Evaluation of Stepped-Lap Adhesive Joints Subjected to Static Tensile Loadings." *International Journal of Adhesion & Adhesives* 28 (2008): 464-70

[6] Owino, V., "Structural Analysis of Soft-Hard Material Interface in an Ant Neck Joint." *Unpublished master's thesis*. The Ohio State University, Columbus, Ohio (2013)

[7] Hepburn, H., Chandler, H., “Material properties of arthropod cuticles: the arthrodial membranes*.” J. Comp. Physiol*, 109, 177-198. (1976)

[8] Nguyen, V. “Development of a Finite Element Model of an Ant Neck-Joint for Simulation of Tensile Loading.” *Unpublished master’s thesis*, The Ohio State University, Columbus, Ohio.(2012)

[9] Sewry, C. “Paraffin wax embedded muscle is suitable for the diagnosis of muscular dystrophy.” *Journal of Clinical Pathology*. (2002)

[10] Berry, R., Ibbotson, M. “A Three-Dimensional Atlas of the Honeybee Neck. “ *PLOS ONE*. (2010)

[11] Suzuki, T., Matsuzaki, R., Todoroki, A., Mizutani, Y., “Crack growth analysis of a composite / adhesive interface toughened by in-mold surface preparation.” *International Journal of Adhesion & Adhesives*, 36-43, (2013)

[12] M. J. Lee, J. M. Lim & B.C. Lee, “Finite Element Analysis of an Adhesive Joint Using the Cohesive Zone Model and Surface Pattern Design of Bonding Surfaces.” *The Journal of Adhesion*, 89:3, 205-224, (2013)

[13] Dirks, J., Taylor, D., "Fracture toughness of insect wings." *PLOS One* 7 (8), e434111 (2012b)

[14] Gorb, S.N., "Ultrastructure of the Neck Membrane in Dragonflies (Insecta, Odanta)," *Journal of Zoology*, pp.479-494, (2000)

[15] Gorb, S.N., "Armored Cuticular Membranes in Brachycera (Insecta, Diptera)," *Journal of Morphology*, pp. 213-222, (1997)

Appendices

Appendix A: **Using Acrylic Resin to Embed Ant Specimen**

Appendix B: **Using a Milling Machine for Desired Cross-Section**

Appendix C: **Sputter Coating Specimen (Gold)**

Appendix D: **SEM Imaging Tips Using Quanta 200**

Appendix A

Using Acrylic Resin to Embed Ant Specimen

Location: Any available lab with a fume hood or in a well-ventilated area

Procedures

These procedures must be done in a well-ventilated room or under a fume hood.

1. Have ant specimen prepared, making sure they are well cleaned and dried (refer to appropriate protocol).
2. Be sure to use safety gloves for the following procedures.
3. Pour desired amount of acrylic plastic casting (usually larger bottle) into mixing tub. This will be the basis of the liquid resin.
4. The following table can be used to calculate the amount of hardener that would be required for a particular part thickness.

For every one ounce of liquid resin:

Thickness	Hardener Required
1/8” ~ 1/4“	8 ~ 10 drops
1/4” ~ 1/2“	4 ~ 6 drops
1/2" ~ 1”	3 ~ 4 drops
1” ~ 2”	3 drops

5. In general, the maximum 10 drops was used to cast the specimen.
6. Mix liquid resin and hardener thoroughly in mixing tub.

7. Pipette mixture into Eppendorf tubes, half to three-quarters of the way to the top.
8. Using tweezers, add one specimen to one prepared tube at varying desired angles.
9. Carefully add final layer of mixture over top specimen, completely embedding body in acrylic resin.
10. Repeat for all desired specimen.
11. Leave under fume hood overnight.
    a. Wait at least 48 hours before attempting to machine. Acrylic must be completely hardened.

Required Materials

- Acrylic Resin from Electron Microscopy Sciences (www.emsdiasum.com)
    - Acrylic Plastic Casting: Catalog no. 24210-01
    - Hardener for Acrylic Plastic Casting, Series 24210-H
- Multiple 1.5 mL Eppendorf tubes (one per ant)
    - Useful to have a box to hold tubes (10x10)
- Disposable mixing tub
- Disposable pipettes or similar

Additional Notes

- One unit of hardener will convert one pound of liquid resin into a solid form.
- Thickness of casting will determine ratio of hardener to resin.

- Temperature of room and resin will control the setting time.
- One ounce of resin poured into mold at depth 1/8" ~1/4" will gel in 20~30 minutes at room temperature when mixed with 10 drops of hardener.
- These should harden within 2~3 hours or overnight.

Appendix B

Using a Milling Machine for Desired Cross-Section

Point of Contact: Walter Green, Student Shop Supervisor, MAE OSU

Email: green.758@osu.edu

Location: Student Machine Shop, Scott Lab W299

Procedures

Read through entire protocol before arriving at shop.

1. Have specimen embedded in hardened acrylic resin (refer to appropriate protocol).
    a. Be sure specimen is **completely** dry throughout. Acrylic needs to have been hardened for at least 48 hours.
2. Choose specimen and mark the angle of the desired cut.
3. At an available milling machine, use the vice to grip the specimen at desired angle.
    a. Be sure not to "gorilla"-tighten, but enough to grab the acrylic through the Eppendorf tube.
4. First use 1/8" end mill (available at shop) to cut down to the ant body.
    a. Speed: Fast, approximately 3000 RPM
    b. Take 50~100 thou off at a time until the tool nears the body of the ant.
5. Use air hose as necessary to blow off any excess acrylic chips.

6. Change to 1/16” or 1/32” end mill, depending on size of ant. Carefully machine through specimen body until the tool nears the surface of the neck. Take no more than 10 thou off at a time.
    a. For Carpenter Ants, 1/16” sufficed for this step. For smaller ants, 1/32” may be recommended.
7. Coming down to the specimen neck region, change tool to 1/64” end mill taking no more than 3 thou off at a time. Work around neck region until desired cross-section is exposed.
    a. Speed: As fast as the machine would reasonably go (~3300 RPM)
    b. Check using light and scope to check general neck exposure.
8. Once desired cross-section is cut, turn part upside down to machine off bottom tip of Eppendorf tube. An 1/8” end mill will suffice for this step.
    a. Careful not to crush the ant out of the acrylic resin at this step, as it will be facing down.
9. Once machined, use a knife to pry out the acrylic from the remaining Eppendorf tube.
10. Store in a dust-free location.

Special Tooling Required (unavailable at shop)

- Accupro Square End Mills Mill Diameter
    - (Inch): 1/64 Mill Diameter (Decimal Inch): 0.0156
        - (MSC Part #: 62773213)
    - (Inch): 1/32 Number of Flutes: 3

        - (MSC Part #: 00037630)
- Atrax Square End Mills Mill Diameter
    - (Inch): 1/16 Number of Flutes: 3
        - (MSC Part#: 85330041)

Additional Notes

- Safety First! Be sure to have safety glasses at all times. No open-toed shoes. Take off all jewelry including watches. When applicable, hair must be tied up in a bun. No cell-phone usage inside the machine shop.
- Undergraduate students who have taken ME2900 are allowed to use this shop. Graduate researchers must fill out additional forms. When uncertain, speak to shop supervisor first.
- Machining is a very time consuming process. Be sure to arrive at shop well before closing time. Allot at least 45 minutes **per specimen** to account for both setup and cutting.

Appendix C

Sputter Coating Specimen (Gold)

Point of Contact: Cameron Begg, Senior Research Assoc-Engineer, MSE OSU

Email: begg.4@osu.edu

Location: Center for Electron Microscopy and AnalysiS (CEMAS)

1305 Kinnear Rd, Columbus, OH 43212

Procedures

Updated version of these procedures could be available at CEMAS site.

1. With safety gloves and forceps, carefully place specimen onto coating platform.
    a. The glass cylindrical wall is not necessarily attached to lid, so careful when lifting.
2. Close lid.
3. Be sure gas is initially closed on the adjustable knob.
4. Check to make sure gas line is turned on and available.
5. Separate machine on the floor has a clear-coated button. This is for creating a vacuum in the chamber. Turn button on and wait a few seconds for it to start up.
6. Turn on power for coater.
7. Using the adjustable knob, shift back and forth x3 to let air out by letting the Argon gas in to the chamber.

8. Push down the Test button to see if the reading is <5 mA. If not, continue to wait.
9. Once the Test reads <5 mA, check to make sure the timer is set to ~60 seconds.
10. While holding the Test button, hit Start. Then let go both buttons and allow the sputter coating to take place for ~60 seconds.
11. During the coating process, adjust the knob so it stabilizes at around 15 mA.
12. Once completed (the machine will turn off), power off all equipment. Do not forget to shut the gas pipe off as well.
13. Once completed, pull up the knob on top of the lid to release gas. The lid is now free to be removed.
14. Take samples out; check to make sure the coating is even across the sample.

Additional Steps – In the Case of No Aluminum SEM Pin Studs

This will be in the case where the specimen is embedded in acrylic. Because the specimen is not directly in contact with a conductive material (such as in the case of SEM studs), additional steps must be taken before samples can be placed in the SEM Machine for imaging.

15. Using the included brush, add Colloidal Graphite to the sample by painting one single streak from the top (gold coated surface) and along the side of the acrylic wall.
    a. This will create a connection from the conductive gold layer to the side of the acrylic for a successful SEM imaging.

16. Place in drying oven (could be located in separate room) at 50 degrees Celcius and leave for approximately 10 minutes.
17. After 10 minutes, check to make sure colloidal graphite is dry. The sample is now ready to be imaged in the SEM machine.

Required Materials

- Prepared specimen
- Safety gloves
- Forceps/Tweezers
- Dime (optional – see below)
- Colloidal Graphite (sometimes available at CEMAS)

Additional Notes

- A dime could be used to check evenness of gold coating by including a dime on coating platform along with specimen (Step 1). At Step 14, the dime can be used to determine the evenness of coating.

Appendix D

SEM Imaging Tips Using Quanta 200

Point of Contact: Cameron Begg, Senior Research Assoc-Engineer, MSE OSU

Email: begg.4@osu.edu

Location: Center for Electron Microscopy and AnalysiS (CEMAS)

1305 Kinnear Rd, Columbus, OH 43212

Guidelines

- Schedule training session through Cameron Begg or appropriate supervisor for Quanta 200.
    - Be sure the sample is prepped and sputter coated (refer to appropriate protocol).
- Watch training video on CEMAS website for the Quanta 200 before arriving for training.
- Read over **Using the Quanta-Quick Start Notes** (attached below)
- For scheduling and reserving time slot for the Quanta 200, use the Facility Online Manager (FOM) on the CEMAS website.

Quick Overview of Procedures

1. Put on safety gloves to prevent skin oil from transferring to machine.
2. Green light indicates that the chamber is under vacuum.
3. On the computer, click Vent → Yes.
4. Wait for few moments while air is released into the chamber.

    a. The indicator color on the screen will change from Green to Red when it is ready to put the sample in.
5. Pull door steadily and straight out. Do not yank, as it could hurt the door of the machine.
6. Place sample into stage.
    a. If using the Aluminum SEM pin studs, place the stud into the appropriate mount.
    b. If not using Aluminum SEM pin studs, be sure to use appropriate diamond-shaped spring-loaded mount to grip the acrylic, making contact with the colloidal graphite.
7. Check height with height gauge.
    a. Important step, otherwise could hurt the machine if the sample height is too tall!
8. Gently close the door and press door closed.
9. While pressing door closed, click Pump on the computer.
10. Wait for the indicator lamp to turn Green (the sample is now under vacuum).
11. Have the following settings for ideal image capturing:
    a. 15kV
    b. Everhart-Thornley Secondary Electron Detector
    c. Spot Size = 4.0
12. One settings are set and the sample is ready to be imaged, click HV
13. Check to make sure emission current is approximately 100 μA.
14. Click the quadrant to focus on.

a. Be sure it is set to Detector: Everhart-Thornley ("Det ETD")

15. Pause button on the tool bar will start and stop the quadrant.
16. Contrast button will start auto-contrast.
17. Can double click on Map (black cross) to move to desired coordinate.
    a. Can also manually input coordinates by [x,y, "Goto"]
18. Can change speed from slow to fast by changing from Turtle to Hare.
19. Press -/+ for magnification adjustments.
20. Right click button can be used for focus.
21. Press F5 on keyboard for Whole Screen.
22. Double click on image label to specify image title.
23. Click Camera to freeze and render image.
    a. This will allow user to File → Save As… to keep image.
24. When image capturing is complete, click Vent → Yes and follow similar instructions to remove sample.
25. At the end of SEM session, be sure to repeat Step 9 and 10.
    a. The chamber should stay in vacuum to prevent any dust particles from entering chamber while machine is not in use!

Required Materials

- Appropriate mount(s), should be available in Quanta 200 imaging room
- Safety gloves
- Forceps

Additional Notes

- Be sure to notify Cameron Begg or appropriate staff member if anything seems out of the ordinary or if unsure how to continue with any step.
- Don't forget to sign in and sign out using FOM on the computer for the scheduled times.

Using the Quanta – Quick Start Notes.

If you need to Log on: Username = "Username" and Password = "Password"

Click Vent then "OK" (Vacuum status indicator (VSI) changes Green→Yellow→Red)

Insert, remove or change sample. (Refer to SEM stage movie.) ***Check sample height!***

Click in lower right quadrant (TV camera inside) and click ▎▎ to make it active (or F6)

Use scroll wheel – click, hold, drag up or down, to move Z in lower R quadrant.

Hold chamber door firmly closed. Click on Pump (VSI changes Red→Yellow→Green)

Select High Voltage (HV range = 0-30keV) and Spot Size (electron beam current = 0-7)

Click HV button. Wait for filament to saturate (~100μA)

Click in another quadrant to make it active. (Blue base)

Select Detector (ETD=secondary; SSD=backscatter)

Select picture resolution from pull-down menu:

512x442
1024x884 (used normally)
2048x1768

Click auto contrast/brightness – top left icon (or F9) – or use manual slider controls.

Plus/minus (+ -) keys on the numeric keyboard double or halve the magnification.

Select a low magnification. Click stage map to center sample in X and Y. (or CNTRL+0)

Use scroll wheel – click, hold, drag mouse – to drive around. Or turn stage motor knobs.

Double clicking anywhere on the sample image brings that point to the center.

Focus with R mouse button. ***When accurately focused*** couple Z->FWD (Shift+F9).

Stigmate image using: Shift+R mouse button. Change scan rate: turtle – + hare.

Some more short cuts:
F1 – help F11 – auto focus CNTRL+ 0 (zero) – drive to center
F2 – Snapshot, which does a slow scan then pause. (Same as Integrate 1)
F3 – Waveform monitor "Videoscope". (This is the [green] picture wave signal.)
F5 – Toggles active quadrant (blue bottom bar) to full screen or back to 4 quadrants.
F7 – Reduced area scan F9 – Auto contrast/brightness
Shift+F11 – auto stigmation Shift+F12 – scan rotation
Save data in your own folder. File name extension _### (CNTRL+S)

C Begg JAN2015